

## Exploring the flavor content of light and heavy-light pseudoscalars

R. M. Moita,<sup>1</sup> J. P. B. C. de Melo,<sup>2</sup> K. Tsushima,<sup>2</sup> and T. Frederico<sup>1</sup>

<sup>1</sup>*Instituto Tecnológico de Aeronáutica, DCTA, 12228-900 São José dos Campos, Brazil*

<sup>2</sup>*Laboratório de Física Teórica e Computacional - LFTC,  
Universidade Cruzeiro do Sul and Universidade Cidade de São Paulo (UNICID)  
01506-000 São Paulo, Brazil*

(Dated: November 22, 2021)

The electroweak properties of light and charmed  $D$  and  $D_s$  pseudoscalar mesons are investigated within a unified covariant constituent quark model. The quark-antiquark-meson vertices are assumed to have a symmetric form by the exchange of quark momenta, which is successful in describing the light pseudoscalar meson properties. The flavor decomposition of the elastic electromagnetic form factors, electromagnetic charge radii, and weak decay constants are calculated. Based on the results a discussion on the SU(3) and SU(4) symmetry breaking is made and a comparison with the pion and kaon properties to highlight the Higgs contribution to the structure of these mesons.

### I. INTRODUCTION

The interplay between dynamical and explicit chiral symmetry breaking in quantum chromodynamics (QCD), drives the properties of the heavy-light pseudoscalar mesons, like  $D$  and  $D_s$ , where dressing of the light quarks comes together with the mass of the heavy partner from the coupling to the Higgs boson. The consequence of the dynamical chiral symmetry breaking is the dressing of the light quarks ( $u$ ,  $d$ ,  $s$ ) and the Goldstone boson nature of the pion and kaon (see e.g. [1, 2]), while in heavy sector the charm quark basically acquires its mass from the Higgs coupling, breaking badly the SU(4) flavor symmetry, separating the Goldstone bosons formed by  $u\bar{d}$  and  $u\bar{s}$  from the  $c\bar{d}$  and  $c\bar{s}$  pseudoscalars (see e.g. [3, 4]).

The evolution of the structural properties of the pseudoscalar mesons within the SU(4) multiplet allows to study the competition between the two mass generation mechanisms, as the constituent quark masses change from a couple of hundreds of MeV, of the order of  $\Lambda_{QCD}$ , to the GeV scale. Each meson encodes the full complexity of QCD in Minkowski space, namely its wave function, for example in the light-front (LF), is spread out over an infinite set of Fock-components [5], while by itself the dressed quark degree of freedom encodes such rich structure and it is considered a building block, since the primordial

era of studies of the strong interaction. Nowadays, QCD studies of mesons are far beyond such naive representations with several groups performing lattice (LQCD) calculations over the world. Also, the dressing of light quarks, gluons and ghosts have been computed within LQCD (see e.g. [6]) strengthening the concept of effective quark and gluon degrees of freedom as the building blocks in phenomenological descriptions of hadrons. On the other hand the heavy quarks are barely dressed by gluons, and the Higgs coupling being the dominant effect to acquire their masses.

The well separated mass scales of the light and the charm quarks should manifest in the heavy-light meson internal structure, as already recognized long ago (see e.g. [7, 8]). The combined study of mesons, where the largest component in their wave functions are the non-exotic ones, namely a  $q\bar{q}$ , formed by a dressed light quark and antiquark or a heavy-light  $q\bar{q}$  pair, should allow to follow the transition in the internal structure when a light quark is substituted by a heavy one. In the extreme situation where the heavy mass tends to infinity, the heavy quark in the  $q\bar{q}$  valence component is placed at the center of mass of the meson, while the light quark explores the confining QCD interaction. The pseudoscalar mesons radically change from the Goldstone boson nature of the pion and kaon, associated with dynamical symmetry

breaking, to for example  $D$  and  $D_s$ , where the chiral symmetry is explicitly broken. Such physical transition should be manifested in the structure of these mesons, and in particular in their charge distribution. In the heavy quark limit part of the charge should be distributed at the short-range, while an another part at larger distances, while for the pion and kaon, both the quark and antiquark should bring somewhat similar charge distributions, apart the individual charge carried by each constituent. This sharp modification in the structure of the light-light to the heavy-light pseudoscalars should be reflected in the elastic electromagnetic (EM) form factors, and in particular in their flavor decomposition.

Experimental information on the EM form factors of the pion and kaon are available in Refs. [9–13] and [14, 15], respectively. Furthermore the charge radii of the pion and kaon are quite well determined to be, respectively,  $r_\pi = 0.672 \pm 0.08$  fm and  $r_K = 0.560 \pm 0.03$  fm (see [16] and references therein). However, it is still missing experimental information on the elastic EM form factors of the charged  $D$  and  $D_s$  mesons, which would be essential to address the structural modifications moving from Goldstone bosons to the heavy-light pseudoscalars. On the other side, ab-initio calculations of the  $D$  and  $D_s$  charge radii at the physical pion mass point are not yet available, although some results were obtained within a 2+1 flavor LQCD [17] for pion masses from 300 up to 700 MeV and with twisted boundary conditions [18] for pion masses of 300 and 315 MeV. The extracted charge radius were found around 0.4 fm for the  $D^+$  and somewhat smaller for the  $D_s^+$ , indicating the decrease in the size of these mesons with respect to the charged pion and kaon, as follows from the Higgs coupling to the heavy quarks in opposition to the light ones acquiring dynamically their masses. The performed flavor decomposition of the charge radius clearly supports the physical picture outlined before. Additionally, the EM form factors and the corresponding flavor decomposition for the  $D^+$  up to 1.5 GeV<sup>2</sup> [17] and for  $D^+$  and  $D_s^+$  below 1.2 GeV<sup>2</sup> were computed within LQCD [18]. It is of note that the scarce information of the EM structure of the pseudoscalar mesons is contrasted by the knowledge of the weak decay constants from the experiments and LQCD calculations (see e.g. [16]), which is an important piece of information of the meson valence wave function at short distances, and necessary to be taken into account by phenomenological models.

The above discussion featuring the evolution of the pseudoscalar meson structure from light to heavy-light

mesons as represented by their charge distributions, motivates our study of  $\pi^+$ ,  $K^+$ ,  $D^+$  and  $D_s^+$  within a common and covariant framework with a minimum number of scale parameters, besides the constituent quark masses, all embody in a Bethe-Salpeter (BS) amplitude model. It corresponds to the matrix element of an interpolating operator between the vacuum and the meson state which is built with a minimum number of field operators characterized by the meson quantum numbers [19]. The BS model has a constituent quark and antiquark and a pseudo scalar vertex with one scale parameter, in a generalization of the model proposed in [20], applied with success to compute the pion electroweak properties, and later on used to study the kaon and  $D^+$  electromagnetic form factors [21, 22]. Furthermore, the projection of the  $q\bar{q}$  BS amplitude to the LF gives the valence component of the wave function (see e.g. [23, 24]), which allows one to explore the valence quark momentum distributions (see e.g. [25] and [26]).

In the present work, the BS amplitude model [20] is applied to compute the EM form factors of  $\pi^+$ ,  $K^+$ ,  $D^+$  and  $D_s^+$ , as well as their flavor decomposition, via the Mandelstam formula [27], represented by the triangle Feynman diagram. The model has constituent quarks  $u$ ,  $d$ ,  $s$  and  $c$ , with fixed masses and one individual scale parameter fitted to the well known value of each meson decay constant. The model is covariant and conserves the EM current, as the constituent quarks are point like, with a bare current, which trivially satisfy the Ward-Takahashi identity [19]. In addition, the decay constant is computed from the antialigned quark spin component of the LF valence wave function, which is derived from the BS amplitude model.

In sect. II, an analytical form for the Bethe-Salpeter amplitude in terms of constituent quarks for the pseudoscalars,  $\pi^+$ ,  $K^+$ ,  $D^+$  and  $D_s^+$  is proposed within a unified covariant model, and from that the weak decay constant is derived, and its association with the antialigned quark spin component of the valence LF wave function is presented. In sect. III, the electromagnetic current for the elastic process is constructed, the flavor decomposition of the elastic electromagnetic form factors is derived, and the method for treating numerically the loop integrations with LF technique is discussed. The results for the static electroweak observables are provided in sect. IV, and discussed in comparison with LQCD calculations and other models. The electromagnetic form factors from our model are discussed in sect. V and compared with the vector meson dominance model and with experimental data

for the pion and kaon, while for  $D^+$  and  $D_s^+$  with LQCD results. The work is closed in sect. VI with a summary of the main results.

## II. THE COVARIANT FRAMEWORK

### A. Quark-meson spin coupling: effective Lagrangian

We adopt here a simple scheme to build the spin coupling of the quark-antiquark pair to build the meson starting from an effective Lagrangian. Note that, later on a meson vertex will be introduced carrying a mass scale dictated by the weak decay constant.

$$M_{SU(4)} = \frac{1}{\sqrt{2}} \begin{pmatrix} \frac{\pi^0}{\sqrt{2}} + \frac{\eta}{\sqrt{6}} + \frac{\eta_c}{\sqrt{12}} & \pi^+ & K^+ & \bar{D}^0 \\ \pi^- & -\frac{\pi^0}{\sqrt{2}} + \frac{\eta}{\sqrt{6}} + \frac{\eta_c}{\sqrt{12}} & K^0 & D^- \\ K^- & \bar{K}^0 & -\sqrt{\frac{2}{3}}\eta + \frac{\eta_c}{\sqrt{12}} & D_s^- \\ D^0 & D^+ & D_s^+ & -\frac{3\eta_c}{\sqrt{12}} \end{pmatrix}, \quad (2)$$

is the SU(4) pseudoscalar meson field matrix [29–31].

In particular, the positively charged pseudo-scalar mesons which we focus in this study are selected from the SU(4) meson matrix through the traces

$$\begin{aligned} \pi^+ &= Tr [M_{SU(4)} \lambda_{\pi^+}], \quad K^+ = Tr [M_{SU(4)} \lambda_{K^+}], \\ D^+ &= Tr [M_{SU(4)} \lambda_{D^+}], \quad D_s^+ = Tr [M_{SU(4)} \lambda_{D_s^+}], \end{aligned} \quad (3)$$

where the flavor matrices are given by:

$$\begin{aligned} \lambda_{\pi^+} &= \frac{1}{\sqrt{2}}(\lambda_1 + i\lambda_2), \quad \lambda_{K^+} = \frac{1}{\sqrt{2}}(\lambda_4 + i\lambda_5), \\ \lambda_{D^+} &= \frac{1}{\sqrt{2}}(\lambda_{11} - i\lambda_{12}), \quad \lambda_{D_s^+} = \frac{1}{\sqrt{2}}(\lambda_{13} - i\lambda_{14}), \end{aligned} \quad (4)$$

and the corresponding physical mesons are indicated by the subindices.

### B. Bethe-Salpeter amplitude model

The effective Lagrangian from Eq. (1), is associated to a meson vertex without structure and point-like, introduced only to guide us in a practical form to build both the spin and favor composition of each meson. In what follows, we will allow the meson vertex to have an extension, represented by a scalar function to

We start by coupling the quark to the pseudoscalar meson field within the SU(4) flavor symmetry scheme, which is expressed by the following effective Lagrangian:

$$\mathcal{L}_{\mathcal{I}} = -i g \bar{\Psi} M_{SU(4)} \gamma^5 \Psi \equiv -i \frac{g}{\sqrt{2}} \sum_{i=1}^{15} (\bar{\Psi} \lambda_i \gamma^5 \Psi) \varphi^i, \quad (1)$$

where  $g$  is a coupling constant,  $\lambda_i$  ( $i = 1, \dots, 15$ ) are the SU(4) Gell-Mann matrices [28],  $\varphi^i$  is the Cartesian components of the pseudoscalar meson fields, the quark field is  $\Psi^T = (u, d, s, c)$  ( $T$ : transposition) decomposed in its quark-flavor components and

keep the covariance of the model. In this way, the Bethe-Salpeter amplitude model for the pseudoscalar mesons considered in this study is given by:

$$\Psi_M(k, p) = S_q(k) \gamma^5 g \Lambda_M(k, p) \lambda_M S_q(k - p), \quad (5)$$

where the constituent quark propagator is

$$S_q(k) = i[\not{k} - \widehat{m}_q + i\epsilon]^{-1}, \quad (6)$$

and the quark constituent mass matrix is diagonal,

$$\text{diag}[\widehat{m}_q] = [m_u, m_d, m_s, m_c].$$

The vertex function for the pseudoscalar mesons,  $M = (\pi, K^+, D^+, D_s^+)$ , adopted in the present work is

$$g \Lambda_M(k, p) = \frac{C_M}{k^2 - \mu_M^2 + i\epsilon} + [k \rightarrow p - k], \quad (7)$$

which generalizes the model proposed in Ref. [20] for the pion and the kaon [22] to the heavy-light case. The model assumes that the infrared (IR) dynamics of QCD is translated to the mass scale,  $\mu_M$ , for each pseudoscalar meson in the SU(4) flavor multiplet. The ultraviolet (UV) physics is reflected in the analytic form of the vertex function. The constant  $C_M$  also

depends on the meson and it is determined by the covariant normalization of the BS amplitude:

$$2ip^\mu = N_c \text{Tr} \int \frac{d^4k}{(2\pi)^4} g^2 \Lambda_M^2(k, p) \times \left[ \gamma^5 \lambda_M S_q(k-p) \gamma^\mu S_q(k-p) \gamma^5 \lambda_M^\dagger S_q(k) + \gamma^5 \lambda_M^\dagger S_q(k+p) \gamma^\mu S_q(k+p) \gamma^5 \lambda_M S_q(k) \right], \quad (8)$$

where it was made the simplified assumption that the kernel which would have given origin to this particular vertex function had no dependence on the total momentum, as it is the case of the ladder approximation of the BS equation (see e.g. [26, 32]).

The breaking of the SU(4) symmetry is reflected in the variation of the mass scale  $\mu_M$  and the constituent quark masses as a consequence of both mass generation by the Higgs mechanism and the dynamical chiral symmetry breaking. In particular,  $\mu_M$  is obtained by fitting  $f_M$ , the weak decay constant of the meson  $M$ , for a given set of constituent quark masses.

We observe that the masses of the constituent quarks are associated to an energy scale characteristic of each meson. Such energy scale sets the initial condition for the evolution to obtain the parton distribution function at the different energy scales. For practical applications, it is about 0.5 GeV for the pion (see e.g. [25]), but could change with the meson.

Another comment is appropriate, in order to keep the simplicity of the present phenomenological covariant model, we have adopted the same form of the vertex function for all mesons, which at large momentum behaves as  $1/k^2$ . Such asymptotic form should naively correspond to the situation where the quark and antiquark, exchange a very large momentum, flowing through the one-gluon exchange interaction, that due to the asymptotic freedom dominates the short-distance dynamics of the system (see e.g. Ref. [33]). Of course, we could have other types of vertices, at the expense of introducing more parameters, but we chose to keep the minimal number of scale parameters in this work, namely one per meson.

### C. Weak decay constant

The pion weak decay constant is a measure of the strong interaction dynamical scale, and as such a fundamental requirement that a model satisfies. The

weak decay constant comes as a balance of both short-range and long-range QCD physics to the meson valence wave function, and therefore a necessary constrain in phenomenological models. In the present work, the chosen model satisfies such physical requirement not only for the pion but also for all the pseudoscalar mesons. The pseudoscalar meson decay constants encode relevant physical information on the structure of the pseudoscalar mesons, allowing together with the Cabibbo-Kobayashi-Maskawa (CKM) matrix elements [16, 34] via the leptonic weak decay,  $M \rightarrow l\nu_l$  ( $l$  represents the charged leptons,  $l = e, \mu, \tau$ ) to obtain the weak decay width. In the lowest order it is given by [16, 34]:

$$\Gamma(M \rightarrow l\nu_l) = \frac{G_F^2}{8\pi} f_M^2 m_l^2 m_M \left(1 - \frac{m_l^2}{m_M^2}\right)^2 |V_{q_1 q_2}|^2, \quad (9)$$

where,  $G_F$  is the Fermi coupling constant,  $m_l$  is the lepton mass,  $m_M$  is the pseudoscalar meson mass, and  $V_{q_1 q_2}$  is the corresponding CKM matrix element.

The pseudoscalar meson decay constant,  $f_M$ , is defined through the matrix element of the axial-vector current operator [19, 35],

$$\langle 0 | A_\mu^j | M^k \rangle = i p_\mu f_M \delta^{jk}, \quad (10)$$

where  $A_\mu^j = \bar{q}(0) \gamma_\mu \gamma^5 \frac{\lambda_j}{2} q(0)$  is the axial-vector current. The indices  $j$  and  $k$  identify the isospin (flavor) components of the current operator and pseudoscalar meson.

According to the diagram shown in Fig. 1, we obtain the following expression for the decay constant, with the vertex function from Eq. (7):

$$i p^\mu f_M = N_c \int \frac{d^4k}{(2\pi)^4} \frac{1}{2} \text{Tr} \left[ \gamma^\mu \gamma^5 \lambda_M^\dagger \Psi(k, p) \right], \quad (11)$$

where the pseudoscalar meson is simply labeled by  $M$  and the trace is taken over the spinor and flavor spaces.  $N_c = 3$  is the number of quark colors.

The decay constant  $f_M$  in (11) is evaluated in the rest frame of the pseudoscalar meson,  $p^\mu = (m_M, \vec{0})$ , considering the plus component of the axial-vector current corresponding to  $\gamma^+ \gamma^5 = (\gamma^0 + \gamma^3) \gamma^5$ , and the loop integration is performed with LF momentum. After integration over the LF energy  $k^-$ , we obtain:

$$f_M = \frac{N_c}{4\pi^3} \int d^2k_\perp \int_0^1 dx \psi_M(x, \vec{k}_\perp; m_M, \vec{0}_\perp), \quad (12)$$

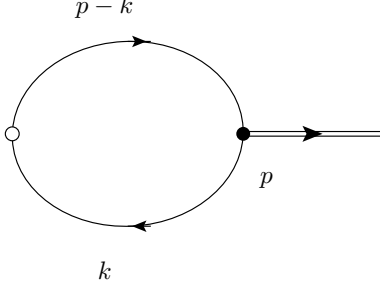


FIG. 1. Diagrammatic representation of the pseudoscalar meson weak decay amplitude.

where  $\psi_M$  is the momentum part of the antialigned quark spin component of the pseudoscalar meson valence wave function, given by:

$$\begin{aligned} \psi_M(x, \vec{k}_\perp; p^+, \vec{p}_\perp) &= \frac{p^+}{m_M} \frac{g C_M}{m_M^2 - \mathcal{M}^2(m_q, m_{\bar{q}})} \\ &\times \left[ \frac{1}{(1-x)(m_M^2 - \mathcal{M}^2(m_q, \mu_M))} \right. \\ &\quad \left. + \frac{1}{x(m_M^2 - \mathcal{M}^2(\mu_M, m_{\bar{q}}))} \right] \\ &\quad + [m_q \leftrightarrow m_{\bar{q}}], \quad (13) \end{aligned}$$

where,  $x = \frac{k^+}{p^+}$ ,  $0 < x < 1$ , and

$$\begin{aligned} \mathcal{M}^2(m_1, m_2) &= \frac{|\vec{k}_\perp|^2 + m_1^2}{x} \\ &\quad + \frac{|\vec{p}_\perp - \vec{k}_\perp|^2 + m_2^2}{1-x} - |\vec{p}_\perp|^2. \quad (14) \end{aligned}$$

Note that, the valence wave function is obtained from the Bethe-Salpeter amplitude (5), by integration over the light-front energy,  $k^-$ , after the instantaneous terms of the quark propagators are dropped out (see Ref [23] for more details). The plus component of the axial-vector current in (11) due to the property  $(\gamma^+)^2 = 0$  kills the instantaneous terms of the quark propagator and the choice of  $\gamma^+ \gamma^5$  to obtain the decay constant selects the valence wave function with antialigned quark spins (see Refs. [24, 26]).

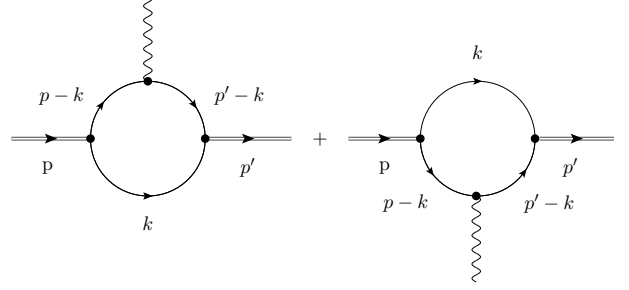


FIG. 2. Feynman diagrams representing the electromagnetic interactions with pseudoscalar mesons for calculating the elastic electromagnetic form factors in the present work, where expressions for each meson are given in Eq.(22).

### III. ELECTROMAGNETIC CURRENT

The quark electromagnetic current operator for the photo-absorption process in a point-like constituent quark is defined by,

$$j^\mu = \frac{2}{3} \bar{u} \gamma^\mu u + \frac{2}{3} \bar{c} \gamma^\mu c - \frac{1}{3} \bar{d} \gamma^\mu d - \frac{1}{3} \bar{s} \gamma^\mu s \quad (15)$$

where  $u, d, s$  and  $c$  are the quark fields. In the flavor space

$$\text{diag}[\widehat{Q}] = [e_u, e_d, e_s, e_c] = [2/3, -1/3, -1/3, 2/3],$$

is the charge operator defined by a diagonal matrix.

The matrix element of the electromagnetic current for each meson is obtained from the Mandelstam formula represented by the Feynman diagrams depicted in Fig. 2 (c.f. Hutaeruk et al. [36]):

$$\begin{aligned} \langle p'; M | j_1^\mu | p; M \rangle &= -i N_c \int \frac{d^4 k}{(2\pi)^4} g \Lambda_M(k, p') g \Lambda_M(k, p) \\ &\times \text{Tr} \left[ \gamma^5 \lambda_M S_q(k-p) \widehat{Q} \gamma^\mu S_q(k-p') \gamma^5 \lambda_M^\dagger S_q(k) \right], \\ \langle p'; M | j_2^\mu | p; M \rangle &= -i N_c \int \frac{d^4 k}{(2\pi)^4} g \Lambda_M(k, p') g \Lambda_M(k, p) \\ &\times \text{Tr} \left[ \gamma^5 \lambda_M^\dagger S_q(k+p') \widehat{Q} \gamma^\mu S_q(k+p) \gamma^5 \lambda_M S_q(k) \right], \quad (16) \end{aligned}$$

where the trace is performed over the Dirac and flavor indices, and the total microscopic current is

$$\langle p'; M | j^\mu | p; M \rangle = \langle p'; M | j_1^\mu | p; M \rangle + \langle p'; M | j_2^\mu | p; M \rangle. \quad (17)$$

Note the above expression contains the two diagrams shown in Fig. 2, and they are written in flavor space

and represent the photon being absorbed by each quark of the meson.

The space-like elastic electromagnetic form factor is extracted by equating the covariant expression (16) to the macroscopic formula of the current:

$$\langle p'; M | j^\mu | p; M \rangle = (p'^\mu + p^\mu) F_M(q^2), \quad (18)$$

where  $q = p' - p$  is the momentum transfer and  $F_M(q^2)$  is the elastic electromagnetic form factor.

We point out that the normalization constant  $C_M$  appearing in the vertex function (7) is determined by  $F_M(0) = 1$ , i.e. the form factor normalization. In addition, the mass scale,  $\mu_M$ , is fitted to reproduce the experimental weak decay constant. The constituent quark mass values ( $m_q$ ) are chosen according to previous studies [20, 22, 37] with similar covariant models.

### A. Flavor decomposition

We can separate the individual contribution from each quark in Eq. 16 by writing the two traces as the sum of two terms: one associated with the photon being absorbed by the quark with charge  $+2/3$ ; and other one corresponds to the antiquark with charge  $+1/3$ . Therefore, we have that for the sum of the two traces:

$$\text{Tr}[\ ] = 2 \left( \frac{2}{3} \Delta_{a\bar{b}a}^\mu + \frac{1}{3} \Delta_{\bar{b}a\bar{b}}^\mu \right), \quad (19)$$

which can be rewritten simply as:

$$\Delta_{aba}^\mu = \text{Tr} [\gamma^5 S_q^a(k-p) \gamma^\mu S_q^a(k-p') S_q^b(k) \gamma^5], \quad (20)$$

the same as (16)  $j_1^\mu$ , where the diagonal matrix element of the quark propagator is  $S_q^a$  for flavor  $a$ . The photon probes in each case the quark or antiquark labeled  $a$  in the first term and  $\bar{b}$  in the second term of Eq. (19), corresponding to the quarks ( $u$  or  $c$ ) and to the antiquarks ( $\bar{d}$  or  $\bar{s}$ ), respectively.

Therefore, the matrix element of the current can be decomposed in the quark flavor content according to:

$$\begin{aligned} \langle p'; M | j^\mu | p; M \rangle &= -2iN_c \int \frac{d^4k}{(2\pi)^4} g\Lambda_M(k, p') g\Lambda_M(k, p) \\ &\times \left( \frac{2}{3} \Delta_{a\bar{b}a}^\mu + \frac{1}{3} \Delta_{\bar{b}a\bar{b}}^\mu \right), \end{aligned} \quad (21)$$

where the photon interacts with the quark  $a$  in the first term and with the antiquark  $\bar{b}$  in the second one.

From that we can write the flavor decomposition of the form factors

$$\begin{aligned} F_{\pi^+}(q^2) &= \frac{2}{3} F_{u\bar{d}u}(q^2) + \frac{1}{3} F_{\bar{d}u\bar{d}}(q^2), \\ F_{K^+}(q^2) &= \frac{2}{3} F_{u\bar{s}u}(q^2) + \frac{1}{3} F_{\bar{s}u\bar{s}}(q^2), \\ F_{D^+}(q^2) &= \frac{2}{3} F_{c\bar{d}c}(q^2) + \frac{1}{3} F_{\bar{d}c\bar{d}}(q^2), \\ F_{D_s^+}(q^2) &= \frac{2}{3} F_{c\bar{s}c}(q^2) + \frac{1}{3} F_{\bar{s}c\bar{s}}(q^2). \end{aligned} \quad (22)$$

In the SU(2) isospin symmetry limit with the  $u$  and  $d$  quark masses being equal, Eq. (21), implies that  $F_{\pi^+}(q^2) = F_{u\bar{d}u}(q^2) = F_{\bar{d}u\bar{d}}(q^2)$ . For  $K^+$ ,  $D^+$  and  $D_s^+$ , respectively the SU(2), S(3) and SU(4) symmetries are broken. By the charge conservation, it is required that

$$\begin{aligned} F_{u\bar{s}u}(0) &= F_{\bar{s}u\bar{s}}(0) = 1, \\ F_{c\bar{d}c}(0) &= F_{\bar{d}c\bar{d}}(0) = 1, \\ F_{c\bar{s}c}(0) &= F_{\bar{s}c\bar{s}}(0) = 1. \end{aligned} \quad (23)$$

The partial quark contributions to each meson form factor becomes different when increasing the momentum transfer, despite the same normalization, as will be shown by our calculations.

### B. LF technique

The calculation of the elastic photo-absorption transition amplitude, Eq. (21), is performed in the Breit frame, with the choice of initial and final meson four-momentum  $p^\mu = (\sqrt{m_M^2 + \frac{1}{4}q_x^2}, -\frac{1}{2}q_x, 0, 0)$  and  $p'^\mu = (\sqrt{m_M^2 + \frac{1}{4}q_x^2}, \frac{1}{2}q_x, 0, 0)$ , respectively. Furthermore, the meson light-front momentum components are chosen as  $p^+ = p'^+ = p^- = p'^-$ ,  $p'_\perp = (q_x/2, 0)$  and  $p_\perp = (-q_x/2, 0)$ , which corresponds to  $q^+ = 0$  fulfilling the Drell-Yan condition [38]. The form factor is obtained from the plus component of the EM current  $J^+ = J^0 + J^3$ , implying in the usage of the quark current associated with  $\gamma^+ = \gamma^0 + \gamma^3$  in Eq. (21), when the relevant Dirac trace is performed, to give:

$$F_M(q^2) = \frac{1}{2p^+} \langle p' | j_M^+ | p \rangle. \quad (24)$$

We should stress that the choice  $\gamma^+$  eliminates the instantaneous terms of the fermion propagators attached to the quark EM current. The loop integration is carried out analytically over  $k^-$ , the light-front

energy, and, after the integrations over  $k^+$  and  $k_\perp$  are performed. Relevant to observe that the choice of the Drell-Yan frame and plus component of the current is enough to eliminate the end-point singularities for this pseudoscalar model (see [20, 39]). However, for frames with  $q^+ \neq 0$ , in order to preserve the full covariance of the model, it is necessary to take into account a nonvalence contribution to the form factor [20, 40].

As a technical remark, the Feynman parameterization could be used alternatively to evaluate the one-loop integrals, keeping the explicit covariance of the model at all steps of the calculations. For our purpose, using the light-cone variables, as we did, or Feynman parametrization should not affect the quantitative results.

#### IV. STATIC ELECTROWEAK OBSERVABLES

The Bethe-Salpeter amplitude model for the  $\pi$ ,  $K$ ,  $D$  and  $D_s$  has for each meson three parameters: the constituent quark masses  $m_q$  with  $q$  from  $\{u, d, s, c\}$  and a mass scale  $\mu_M$  (see Eqs.(5) and (7)). The parameter  $\mu_M$  constrains the model to provide the observed weak decay constant. We work here with six sets of parameters, namely (A,B,C,D,E,F), which respectively correspond to the pseudoscalar mesons ( $\pi^+$ ,  $\pi^+$ ,  $K^+$ ,  $K^+$ ,  $D^+$ ,  $D_s^+$ ), as well as to the different choices of quark masses as given in Table I. The choices of constituent quark masses are: for the light quark mass values of 384 MeV as estimated in [37] (386 MeV was used in [37]) and 220 MeV [20]; the strange constituent mass values of 508 MeV [37] and 440 MeV [22]; and, the charm constituent mass value of 1623 MeV from [37], (see also, the reference [37] for discussions). Note that, the constituent quark mass values for all the models (A), (C), (E), and (F) are from Ref. [37] in the calculation. However, we are assuming that the energy scale associated with each meson should be the same, which may not be valid. We will return to this point later.

The static observables considered, i.e., the charge radius and decay constant, are shown in Table I, where the available experimental data for these two quantities come from Ref. [16], and from [34] for the  $D_s^+$  weak decay constant. In addition, the model binding energy shown in the table is given by:

$$\epsilon_M = m_q + m_{\bar{q}} - m_M > 0. \quad (25)$$

The pion and kaon appear as strongly bound systems with binding energies ranging from about 600

to 400 MeV, respectively, for the best agreement with the charge radius by fitting the decay constants. Both mesons are the Goldstone bosons of the dynamically broken chiral symmetry, and their masses in the chiral limit vanishes according to the Gell-Mann-Oakes-Renner relation, indicating that these states should form strongly bound quark-antiquark systems with constituent quark degrees of freedom.

The Cutkosky rules [19] applied to the triangle diagram (see Fig. 2) taking into account our model for the vertex function, give that the relevant cuts as function of  $m_M$  that have branch points in the regions:

$$\mu_M + m_q - m_M > 0 \quad \text{and} \quad \mu_M + m_{\bar{q}} - m_M > 0. \quad (26)$$

These branch points are also clear in the analytic form of Eq. (13) for the wave function. The minimum value of the position of the branch point is actually the dominant scale that determines the charge radius. From the perspective of the closest value to the continuum, namely corresponding to the minimum value among  $\epsilon_M$  and the branch points in Eq. (26), we can analyse the results for the parametrisations after fitting the decay constants as given in Table I.

For the pion, one finds for sets (A) and (B), 469 and 680 MeV, respectively, for the closest branch point to the continuum. That shows a strongly bound system of constituent quarks, and not surprisingly closer values for the two sets than the binding energies. For the kaon, the sets (C) and (D) present the branching points at 310 and 326 MeV, respectively, that are somewhat closer than considering the comparison only of the binding energies.

For the  $D^+$ , set (E), one realizes that in agreement with the constraint coming from Eq. (26), the value of  $\mu_M \sim m_c$ , and the minimum branch point is actually at 122 MeV, that is associated with the charge radius of 0.505 fm, while for the  $D_s^+$  we find 225 MeV, and a radius of 0.377 fm. The larger value of the  $D_s^+$  branch point and the concomitant decreasing of the radius with respect to  $D^+$  come from the larger value of  $f_{D_s^+}$  and  $m_s$  in comparison to  $f_{D^+}$  and  $m_d$ . Therefore, the quarks in  $D_s^+$  are in a more compact configuration than the corresponding ones in  $D^+$ , and it is expect in general that  $r_{D_s^+} < r_{D^+}$ .

Analogous qualitative explanation of the fact that  $r_{K^+} < r_{\pi^+}$  should be valid. As we will discuss later on, LQCD results obtained using consistent data sets shows that  $r_{D_s^+} < r_{D^+}$  [17, 18], supporting our expectation.

The minimum value of the position of the branch point is actually the dominant scale that determines

TABLE I. Pseudoscalar meson static electroweak observables. The notation for the entries, (A,B,C,D,E,F) respectively correspond to the different model parameters and pseudoscalar mesons for  $(\pi^+, \pi^+, K^+, K^+, D^+, D_s^+)$ . In particular, the results with models B and D are from Ref. [22]. Note that, all the relevant constituent quark mass values for the models A, C, E, and F, are from Ref. [37]. The experimental data come from Refs. [16, 34]. The masses  $m_q, m_{\bar{q}}, \mu_M$ , binding energy ( $\epsilon_M$ ) and decay constant ( $f_M$ ) are given in [MeV]. The charge radius ( $r_M$ ) is given in [fm].

Model/meson	Flavors	$I(J^P)$	$m_q$	$m_{\bar{q}}$	$m_M$	$\epsilon_M$	$\mu_M$	$r_M$	$f_M$	$r_M^{\text{Expt.}}$	$f_M^{\text{Expt.}}$
(A) $\pi^+$	$u\bar{d}$	$1(0^-)$	384	384	140	628	225	0.665	92.55	0.672(8)	92.28(7) [16]
(B)			220	220		300	600	0.736	92.12		
(C) $K^+$	$u\bar{s}$	$\frac{1}{2}(0^-)$	384	508	494	398	420	0.551	110.8	0.560(3)	110(1) [16]
(D)			220	440		166	600	0.754	110.8		
(E) $D^+$	$c\bar{d}$	$\frac{1}{5}(0^-)$	1623	384	1869	138	1607	0.505	144.5		144(3) [16]
(F) $D_s^+$	$c\bar{s}$	$0(0^-)$	1623	508	1968	163	1685	0.377	182.7		182(3) [16] 179(5) [34]

TABLE II. Decay constants and electromagnetic radii of  $\pi^+$  (model A) and  $K^+$  (model C) in the present model, compared with the other works in the literature, as well as the experimental data in particle data group (PDG) [16]. The decay constants are in [MeV], and the charge radius are in [fm].

Reference	$f_\pi^+$	$f_K^+$	$r_{\pi^+}$	$r_{K^+}$	$f_{K^+}/f_{\pi^+}$
This work	92.55	110.8	0.665	0.551	1.196
Maris & Tandy [32]	92.62	109.60	0.671	0.615	1.182
Faessler et al. [41]	92.62	113.83	0.65		1.23
Ebert et al. [42, 43]	109.60	165.45	0.66	0.57	1.24
Bashir et al. [44]	101				
Chen & Chang [45]	93	111			1.192
Hutauruk et al. [36]	93	97	0.629	0.586	1.043
Ivanov et al. [46]	92.14	111.0			1.20
Silva et al. [47]	101	129	0.672	0.710	1.276
Jia & Vary [48]	142.8	166.7	0.68(5)	0.54(3)	1.166
PDG [16]	92.28(7)	110(1)	0.672(8)	0.560(3)	1.192(14)

the charge radius. From the perspective of the closest value to the continuum, namely corresponding to the minimum value among  $\epsilon_M$  and the branch points in Eq. (26).

### A. Pion and Kaon

In Table II we present our results for the pion (A) and kaon (C) charge radii for the sake of comparison with other calculations [32, 36, 41, 44–48]. Our collection of results from the literature is by no means complete, and our intention is just to place our model

with respect to a sample that covers continuum approaches to QCD with Euclidean Schwinger-Dyson and Bethe-Salpeter, phenomenological ones with and without confinement. In the table, we also show the experimental results from [16, 34].

The results obtained with the Euclidean Schwinger-Dyson and Bethe-Salpeter equations with phenomenological kernels that satisfy the axial-vector Ward-identities, having dynamical chiral symmetry breaking in the SU(3) sector were taken from Refs. [32] and [44]. A modern approach along this direction [45] has the quark-antiquark interaction composed by a flavor dependent IR part and a flavor independent UV



TABLE III.  $D^+$  and  $D_s^+$  weak decay constants in [MeV], and the electromagnetic square radii in [ $fm$ ] for various models. Experimental data from [16, 34].

Reference	$f_{D^+}$	$f_{D_s^+}$	$r_{D^+}$	$r_{D_s^+}$	$f_{D_s^+}/f_{D^+}$
This work	144.50	182.70	0.505	0.377	1.26
Faessler et al. [41]	149.20	156.98			1.05
Bashir et al. [44]	155.4	205.1			1.32
Ivanov et al. [46]	145.7	182.2			1.25
Choi [49]	149.2	179.6			1.20
Hwang [50]	145.7(6.3)	189(13)	$0.406_{+0.014}^{-0.012}$	$0.300_{+0.023}^{-0.018}$	1.30(4)
Das et al. [51]			0.510	0.465	
Dhiman & Dahiya [52]	147.8	167.6			1.13
Tang et al. [53]	295(63)	313(67)			1.06(32)
LQCD					
Aubin et al. [54]	142(2)(12)	176(2)(11)			1.24(1)(7)
Follana et al. [55]	147(3)	170(2)			1.16(3)
Chen et al. [56]	143.1(1.6)(1.8)	182.9(0.8)(2.0)			1.28(3)
Carrasco et al. [57]	146.6(2.6)(0.6)	174.8(2.8)(1.0)			1.19(3)(1)
Can et al. [17]			0.371(17)		
			0.390(33)		
Li & Wu [18]			0.402(61)	0.286(19)	
			0.420(82)	0.354(18)	
PDG [16]	144(3)	182(3)			1.26(5)
Ablikin et al. [34]		178.8(2.6)			

part. We also compare with results from a relativistic constituent quark model, which implements a linear realization of chiral symmetry [41].

The solution of the Bethe-Salpeter equation for the Nambu and Jona-Lasinio (NJL) model with proper-time regularization is given in [36]. The results for the covariant confining quark model treated in Euclidean space were reviewed in Ref. [46].

Calculations performed in LF approaches [47, 48] were also presented in Table II. In Ref. [47] a refined light-front phenomenological model for the pion and

kaon elastic form factors, relying on the use of Pauli-Villars regulators in a non-symmetrical form, presents result close to our findings. In Ref. [48], a model with color singlet NJL and confining interactions was studied within basis of light-front quantization.

The pion and kaon are strongly bound systems of constituent quarks in the models presented, and in general they are able to provide reasonable reproduction of their decay constants and charge radii. This is the main feature learned from Table II, and once the decay constant is reproduced in the strongly bound

system the charge radius follows [58, 59].

### B. $D^+$ and $D_s^+$ mesons

The comparison of our results and a selection of models from the literature [41, 44, 46, 49–52] is presented in Table III, together with the outcomes of LQCD calculations [17, 18, 54–57]. In the table we present the charge radii and weak decay constants for  $D^+$  and  $D_s^+$  mesons, as well as the experimental data from Refs. [16, 34], and in particular the ratio  $f_{D_s^+}/f_{D^+} = 1.226(31)(2)(3)$  [16].

The results within Euclidean Schwinger-Dyson and Bethe-Salpeter equation framework with phenomenological quark-antiquark interaction kernel that entails infrared confinement and ultraviolet one-gluon exchange from QCD applied to the heavy-light mesons were taken from Ref. [44]. The calculations within light-cone phenomenological models with confinement come from Refs. [49, 50, 52]. A confining potential model in instant form applied to describe the heavy-light mesons were used in [51]. The results from LQCD for decay constants were taken from Refs. [54, 55], the  $D^+$  charge radius comes from [17] and for  $D^+$  and  $D_s^+$  from [18]. In general, the decay constants are quite close to the experimental values, while for the charge radii there is a spread in the theory results.

Our results for the charge radii,  $r_{D^+} = 0.505$  fm and  $r_{D_s^+} = 0.377$  fm, are somewhat larger than the ones computed within LQCD [17, 18] and the models with confinement [50, 51]. The present model does not have explicit confinement, as the meson is formed as a bound state with about 100 MeV binding energy, and even considering that the decay constants were fitted the charge radii, it is not strongly constrained. Differently from the pion and kaon, the decay constant does not seem to determine definitively the charge radius. We can trace back this behavior to the dominant factor  $m_c/x$  carried by the valence wave function, Eq. (13), to the expression for the decay constant, Eq. (12), as the charm constituent mass is substantially larger than the light quark ones, in other words the heavy quark is close to the center of mass of the system, which corresponds to the region that the wave function is probed in the weak decay amplitude. Therefore, naively it is quite reasonable that the light quark in the BS amplitude is loosely constrained by fitting the decay constant, however its contribution to the charge radius is far more impor-

TABLE IV. Pseudoscalar meson static observables with the masses for  $D$  and  $D_s$  mesons from LQCD ensembles (B1), (C1) used in Refs. [18] to compute the EM form factors; and the present model (E,F) parameters:  $m_c = 1623$  MeV,  $m_u = 384$  MeV,  $m_s = 508$  MeV,  $\mu_{D^+} = 1607$  MeV, and  $\mu_{D_s^+} = 1685$  MeV. The mass and decay constant are given in MeV, while the charge radius is given in fm.

Inputs	(B1)	(C1)	(E,F)
$m_D^+$	1737	1824	1869
$m_{D_s^+}$	1801	1880	1968
Static observ.	(B1)	(C1)	(E,F)
$r_{D^+}$ [18]	0.402(61)	0.420(82)	
$r_{D^+}$	0.347	0.422	0.505
$f_{D^+}$	205.5	170.3	144.5
$r_{D_s^+}$ [18]	0.286(19)	0.354(18)	
$r_{D_s^+}$	0.281	0.312	0.377
$f_{D_s^+}$	243.3	219.4	182.7

tant than the charm one as one can check e.g. in the LQCD calculations [17, 18].

The light quark within the heavy meson can explore larger distances where the QCD infrared physics is relevant and from where the meson gains weight, i.e., the mass is formed, and thus, one should expect a correlation of the charge radius and the actual value of mass of the charmed mesons found within LQCD. In Table IV, we compare the charge radius of  $D^+$  and  $D_s^+$  with the LQCD results from Refs. [18]. For the  $D_s$  meson the LQCD radius increases with the mass and indicates that our result would be compatible, within their uncertainties. For the  $D$ , although there is a slight increase of the radius with the mass, these LQCD results have large errors to make a firm conclusion from the comparison. In the table we also show our calculation for the charge radius changing the mass of the  $D^+$  mesons according to the LQCD values. We observe that the tendency of increasing radius by increasing the  $D^+$  and  $D_s^+$  meson masses as found in the LQCD calculation seems to somewhat reproduced by our model. This feature comes in our model due to the decreasing of the binding energy, which leads to the increase of the meson size. This suggests that the quantum mechanical binding mechanism is somewhat acting in these heavy-light mesons, even though the complexity of the quark confinement

TABLE V. Flavor decomposition of the charge radii of the  $D^+$  and  $D_s^+$  mesons. Comparison with LQCD results from the linear fit (L) and quadratic fit (Q) extrapolating to the physical pion mass from Ref. [17], and from the ensembles (B1) and (C1) used in Refs. [18]

Radius (fm)	LQCD [17]	LQCD [18]	This work
$r_{D^+}$	0.371(17) (L) 0.390(33) (Q)	0.402(61) (B1) 0.420(82) (C1)	0.505
$r_{D^+,c}$	0.226(24) (L) 0.272(29) (Q)	0.17(15) (B1) 0.20(19) (C1)	0.233
$r_{D^+,\bar{d}}$	0.585(57) (L) 0.566(104) (Q)	0.692(61) (B1) 0.718(82) (C1)	0.810
$r_{D_s^+}$		0.286(19) (B1) 0.354(18) (C1)	0.377
$r_{D_s^+,c}$		0.119(50) (B1) 0.222(33) (C1)	0.218
$r_{D_s^+,\bar{s}}$		0.461(12) (B1) 0.545(15) (C1)	0.576

mechanism.

The flavor decomposition of the charge radii of the  $D^+$  and  $D_s^+$  mesons is presented in Table V, where we also compare our model with LQCD results from the linear fit and quadratic fit extrapolating to the physical pion mass given in Ref. [17], and from the ensembles (B1) and (C1) used in Refs. [18]. The flavor contribution to the  $D^+$  and  $D_s^+$  charge radius squared are defined as:

$$\begin{aligned}
 r_{D^+,c}^2 &= 6 \frac{\partial}{\partial q^2} F_{c\bar{d}c}(q^2)|_{q^2=0}, \\
 r_{D^+,\bar{d}}^2 &= 6 \frac{\partial}{\partial q^2} F_{\bar{d}c\bar{d}}(q^2)|_{q^2=0}, \\
 r_{D_s^+,c}^2 &= 6 \frac{\partial}{\partial q^2} F_{c\bar{s}c}(q^2)|_{q^2=0}, \\
 r_{D_s^+,\bar{s}}^2 &= 6 \frac{\partial}{\partial q^2} F_{\bar{s}c\bar{s}}(q^2)|_{q^2=0},
 \end{aligned} \tag{27}$$

and the relations to the meson charge radius are:

$$\begin{aligned}
 r_{D^+}^2 &= \frac{2}{3} r_{D^+,c}^2 + \frac{1}{3} r_{D^+,\bar{d}}^2, \\
 r_{D_s^+}^2 &= \frac{2}{3} r_{D_s^+,c}^2 + \frac{1}{3} r_{D_s^+,\bar{s}}^2.
 \end{aligned} \tag{28}$$

The full charge radii given in Table V are largely dominated by the light quark contribution, and we observe

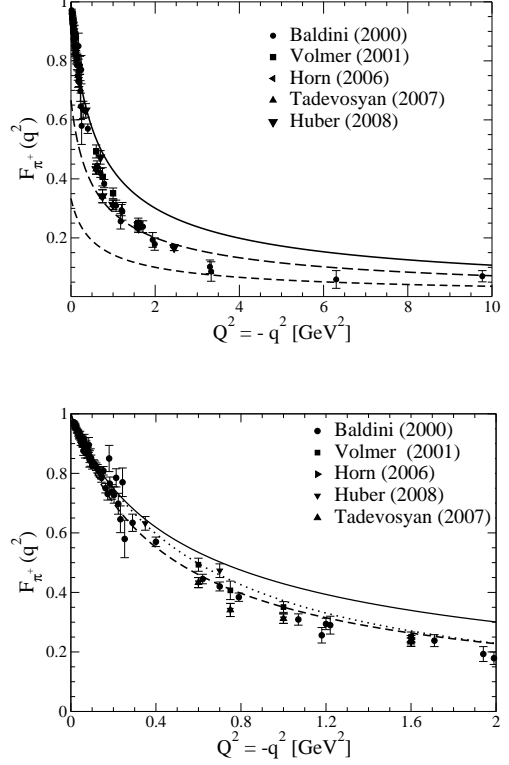


FIG. 3. Pion electromagnetic form factor as a function of  $q^2 < 0$ . Upper panel: Flavor decomposition of  $F_\pi(q^2)$  for the parameter set (A) (see Table I). Pion form factor (solid line),  $u$  contribution -  $e_u F_{u\bar{d}u}$  (dashed line) and  $\bar{d}$  contribution -  $e_{\bar{d}} F_{\bar{d}c\bar{d}}$  (short-dashed line). Lower panel: Comparison between the parameter sets (A) (solid line) and (B) (dashed line) with the VMD model (dotted line) from Eq. (29). Experimental data are from Refs. [9–13].

this property is also shared by the LQCD calculations. The heavy quark predominantly is placed close to the center of mass of the heavy-light meson, while the light one is in the region of about 0.6 - 1 fm distance from the meson center. Amazingly, even being at the confinement region the charge radius contribution from the light quark is quite consistent with the more recent LQCD results from Refs. [18], although we observe the tendency to overestimate these lattice calculations.

## V. EM FORM FACTORS

### A. Pion and Kaon

The extraction of the pion charge form factor from the experimental cross-section for the exclusive pion electroproduction on the proton relies on the dominance of the Sullivan process, due to the pion pole close to the allowed kinematic region for small  $t$ 's [1]. In principle, it is possible to perform exclusive electroproduction of  $K^+$  in experiments on the proton, to extract the form factor at higher momentum transfers [1, 60]. However, in the case of  $K^+$ , there is no recent experimental data for the EM form factor. The experimental data obtained at CERN in 1986, come from the most precise measurement for the  $K^+$  meson [15] that exist up to the present, and what will be used in the study of our model.

We start the discussion of the light pseudoscalar EM form factors based on the vector meson dominance (VMD) model, formulated by Sakurai and others [61–63]. The charge form factors of  $\pi^+$  and  $K^+$  within the VMD description are parametrized by the vector mesons masses  $m_\rho$  and  $m_\phi$ , as:

$$F_{\pi^+}(q^2) = (e_u + e_{\bar{d}}) \frac{m_\rho^2}{m_\rho^2 - q^2}, \quad (29)$$

$$F_{K^+}(q^2) = e_u \frac{m_\rho^2}{m_\rho^2 - q^2} + e_{\bar{s}} \frac{m_\phi^2}{m_\phi^2 - q^2}, \quad (30)$$

where in the space-like region  $Q^2 \equiv -q^2 > 0$ . We assume within the SU(3) flavor symmetry that the coupling constants of the  $\rho$  and  $\phi$  are flavor independent, i.e.,  $g_{\rho,u} = g_{\rho,d} = g_{\phi,s}$ , which implies in the expressions written in Eqs. (29) and (30). From that the ratio between the two contributions to the form factor at  $Q^2 = 0$  are the same as the quark charge ratio, as in our formulation of the form factor for  $K^+$  due to the charge conservation expressed by Eq. (23). As a matter of fact, this is also verified in our model when the charm and light quark contributions are separated in the  $D^+$  and  $D_s^+$  form factors.

Furthermore, at the level of the VMD, we found that the ratio between the quark contributions to  $F_{K^+}(q^2)$  for  $Q^2 \gg m_\phi^2$  is given by:

$$\left. \frac{e_{\bar{s}} F_{\bar{s}u\bar{s}} m_\phi^2}{e_u F_{u\bar{s}u} m_\rho^2} \right|_{(q^2 \gg m_\phi^2)} \rightarrow \frac{1}{2} \frac{m_\phi^2}{m_\rho^2} = 0.86, \quad (31)$$

where the experimental meson masses are used [16]. For comparison, the present model gives  $\simeq 0.56$  (at

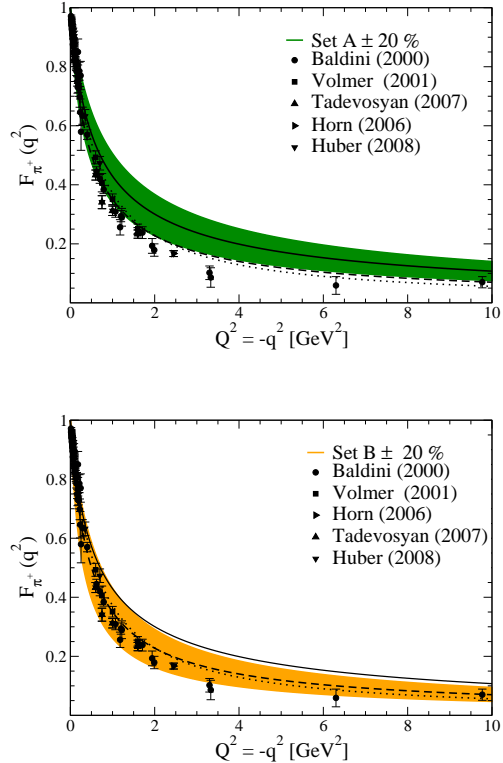


FIG. 4. Pion electromagnetic form factor calculated with variation of the model parameters. Upper panel: band for set (A) with  $\pm 20\%$  variation of the model parameters. Lower panel: band for set (B) with  $\pm 20\%$  variation of the model parameters. In both panels: set (A) (solid line), set(B) (dashed line) and VMD (dotted line). Experimental data are from Refs. [9–13].

10 GeV<sup>2</sup>) with parameters from set (C) (see Tables I and VI).

In Fig. 3, we present the results for the pion EM form factor obtained with the parameter sets (A), (B) (see Table I) and the VMD model in Eq. (29). In both panels the experimental data from [9–13] are also shown. In the upper panel of the figure, the individual quark contributions are shown up to 10 GeV<sup>2</sup> for set (A), and the contributions from the  $u$  and  $\bar{d}$  quarks are in the ratio 2:1, as it should be from the model with SU(2) flavor symmetry.

The comparison between the results for sets (A), (B) and the VMD model is presented in the lower panel of Fig. 3. Note that the set (A) reproduces well the experimental values of  $\pi^+$  charge radius and decay constant, while set (B) performs better at large

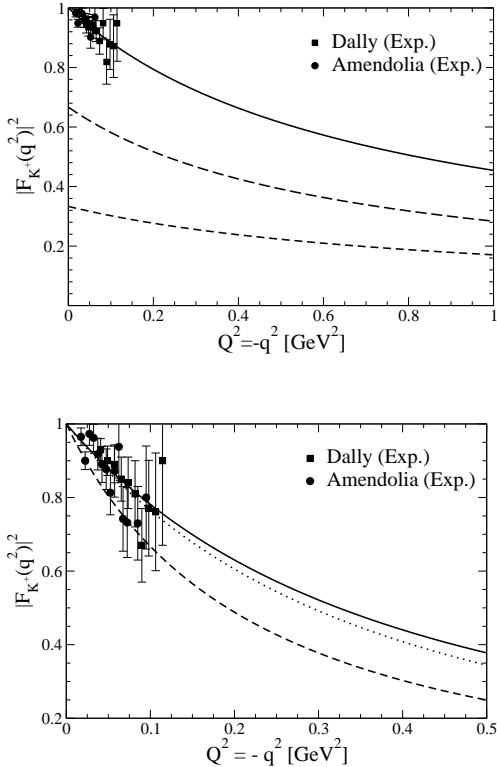


FIG. 5. Kaon electromagnetic form factor as a function  $q^2 < 0$ . Upper panel: kaon form factor (full line),  $u$  contribution -  $e_u F_{u\bar{s}u}$  (dashed line) and  $\bar{s}$  contribution -  $e_{\bar{s}} F_{\bar{s}u\bar{s}}$  (short-dashed line), computed with the parameter set (C) (see Table I). Lower panel:  $|F_{K^+}|^2$ , comparison between the results from parameter sets (C) (full line), (D) (dashed line) and the VMD model from Eq. (30) (dotted line). Experimental data from [14, 15].

momentum transfers, but the charge radius is overvalued (see Table I). However, both sets have form factors with the same analytical behavior at large momentum transfer region, and only their normalizations differ by a couple of tenths of percent. This suggests a limitation in the chosen form of the vertex function to describe the pion charge distribution. Indeed, models with running quark masses and incorporating the asymptotic QCD counting rules are known to perform better with respect to the experimental data (see e.g. [32, 44, 64]).

In order to overcome the limitation of the model, we allowed a  $\pm 20\%$  parameter variation in sets (A) and (B), keeping the pion mass fixed in Fig. 4. This changes both the decay constant and charge radius,

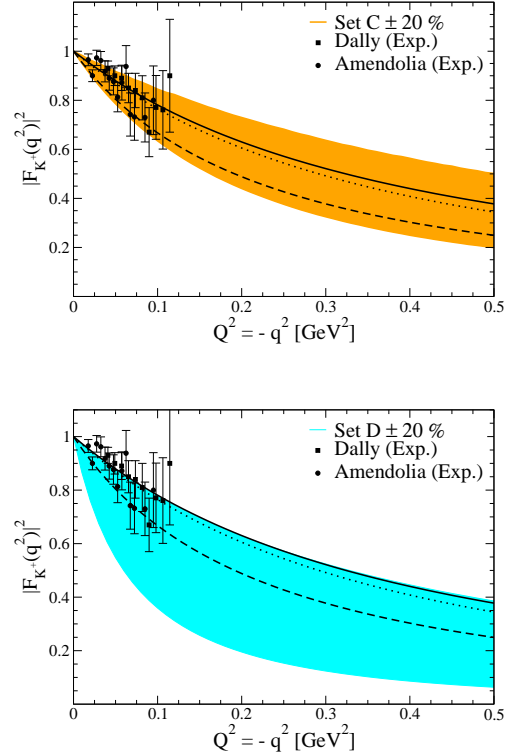


FIG. 6. Kaon electromagnetic form factor square with variation of the model parameters. Upper panel: band for set (C) with  $\pm 20\%$  variation of the model parameters. Lower panel: band for set (D) with  $\pm 20\%$  variation of the model parameters. In both panels: set (C) (solid line), set (D) (dashed line) and VMD (dotted line). Experimental data from Refs [14, 15].

while it allows that results with the variation of set (A) becomes much closer to the experimental data, set (B) produces a band englobing almost all the experimental data. In the chiral limit, where the pion becomes massless the changes in the constituent quark masses and mass scale parameter by a factor  $\lambda$  will give for the new form factor,  $f'_\pi(q^2)$ , the scaling relation:

$$f'_\pi(q^2) = f_\pi(\lambda^2 q^2), \quad (32)$$

and it represents reasonably well the band that one sees in the figure.

A last comment on the pion form factor is in order. The pion and heavy meson energy scales can be different, as we have pointed out earlier. The pion is a strongly bound system of the constituent quarks, and therefore should be associated with a somewhat larger energy scale with respect to the heavy meson ones.

This explains why the pion form factor at large momentum transfers is better reproduced with model B having lighter u and d quarks, in contrast with model A, where the quark mass is appropriate for the heavy mesons.

We present the results for the  $K^+$  form factor in Figs. 5 and 6 obtained with the two sets of parameters (C) and (D) (see Table I). We also compare the results with the VMD model and the experimental data from [14, 15]. We remind that the set (C) presents a charge radius and weak decay constant in agreement with the experimental values. The parameter set (D) reproduces the decay constant but has about 20% difference with the experimental value of the kaon charge radius. In the upper panel of Fig. 5, we show the results obtained with the set C, for the full and the  $u$  and  $\bar{s}$  quark contributions for the kaon form factor. In the figure, it is possible to see, that the SU(3) flavor symmetry is slightly broken, as the ratio  $e_{\bar{s}}F_{\bar{s}u\bar{s}}/(e_uF_{u\bar{s}u}) > 1/2$  for  $Q^2 \neq 0$ . The same feature is also found in the NJL model [36].

In the lower panel of Fig. 5 we compare the results for the kaon form factor in the low momentum transfer region up to  $0.5 \text{ GeV}^2$  obtained with set (C), (D) and the VMD model together with the experimental data [14, 15].

One can see that this data cannot unambiguously resolve between sets (C) and (D), with both somewhat consistent with the experimental results. From Table I, we have that set (C) reproduces the experimental kaon charge radius and it is also consistent with the VMD form factor, therefore taking that into account we could say that it presents an overall better consistency with the data.

In the upper panel of Fig. 6, we examine the effects of a  $\pm 20\%$  variation in the model parameters on the kaon EM form factor using set (C). The band now englobes the experimental data for the form factor. Although, the validity of an analogous scaling property as verified for the pion in Eq. (32) is questionable, as the constituent quark masses, mass scale parameter and binding energy are large enough, a similar band is found as in the pion case. However, the 20% change in the parameters of set (D) keeping the kaon mass fixed as presented in the lower panel of the figure, shows a quite large band. This is due to the fact that decreasing the masses in set (D) by 20% makes the binding energy drops from 166 MeV (Table I) to only 34 MeV, producing a large increase in the radius, and consequently the wide band observed in the figure.

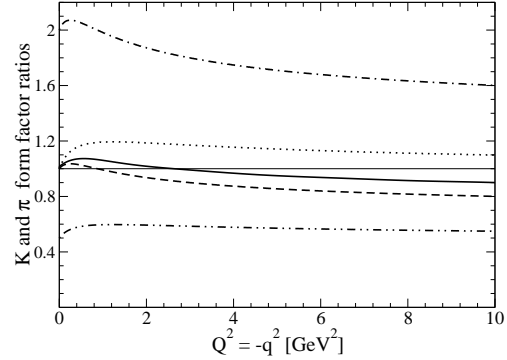


FIG. 7. The electromagnetic form factor ratios for the pion and kaon using sets (A) and (C), respectively. Ratios of flavor contributions to the pion and kaon form factors:  $F_{K^+}/F_{\pi^+}$  (solid line);  $e_uF_{u\bar{s}u}/(e_{\bar{d}}F_{\bar{d}u\bar{d}})$  (dot-dashed line);  $F_{u\bar{s}u}/F_{u\bar{d}u}$  (dashed line);  $F_{\bar{s}u\bar{s}}/F_{\bar{d}u\bar{d}}$  (dotted line);  $e_{\bar{s}}F_{\bar{s}u\bar{s}}/(e_uF_{u\bar{s}u})$  (dot-dot-dashed line). A thin solid line is the reference for the SU(3) flavor symmetry.

The breaking of the SU(3) flavor symmetry is analyzed using the sets (A) and (C) in Fig. 7, where we show several ratios of form factors to evidence such effect in the space-like region. The ratio of the kaon and pion form factors goes above unity at low momentum reflecting the more compact charge distribution of the kaon with respect to the pion one, while at large momentum transfers we observe that the ratio stays below the unity. This can be traced back to the fact that set (A) produces a pion form factor above the experimental data at large momentum transfers, as well as above the VMD results (see Fig. 4), while the kaon form factor for set (C) agrees with the VMD one (see the lower panel of Fig. 5). The VMD model from Eqs. (29) and (30) gives the ratio at large momentum transfers:

$$\frac{F_{K^+}(q^2)}{F_{\pi^+}(q^2)} \rightarrow e_u + e_{\bar{s}} \frac{m_\phi^2}{m_p^2} = 1.24, \quad (33)$$

while QCD for  $Q^2 \gg \Lambda_{QCD}^2$  predicts that [65]:

$$\frac{F_{K^+}(q^2)}{F_{\pi^+}(q^2)} \rightarrow \frac{f_K^2}{f_\pi^2} = 1.42 \pm 0.03, \quad (34)$$

where we have used the experimental value for the decay constant ratio [16]. If we had chosen set (B) for the pion with set (C) for the kaon to compute  $F_{K^+}(q^2)/F_{\pi^+}(q^2)$ , we would have had a value somewhat larger than unity, towards the QCD results, however the model doesn't have the perturbative QCD

dynamics built in, and we do not expect to reproduce Eq. (34) in the asymptotic momentum region. Indeed, emphasizing that our model is to be applicable at low momentum transfers, we computed for  $Q^2 = 200 \text{ GeV}^2$  the product  $Q^2 F_\pi(Q^2)$ , which is already saturated around a value of  $1.96 \text{ GeV}^2$  for set A and  $1 \text{ GeV}^2$  for set B from Table I, while the asymptotic QCD formula  $Q^2 F_\pi(Q^2) \rightarrow 16\pi\alpha_s(Q^2)f_\pi^2$  [65] for  $Q^2 = 200 \text{ GeV}^2$  gives  $\sim 0.1 \text{ GeV}^2$  with  $\alpha_s(Q^2)$  from [16].

In addition, in Fig. 7 the ratios of flavor contributions for the pion and kaon form factors are shown. The ratio of the  $u$  quark contribution to the kaon and pion form factors, denoted by  $F_{u\bar{s}u}/F_{u\bar{d}u}$  follows a similar trend as the ratio of the full form factor, as well as  $e_u F_{u\bar{s}u}/(e_{\bar{d}} F_{\bar{d}u\bar{d}})$  apart the factor 2 from the charge ratio, as for the pion  $F_{u\bar{d}u} = F_{\bar{d}u\bar{d}}$ . At small momentum transfers, we observe that the configuration where photon is absorbed by the  $u$  quark in the pion is somewhat larger than in the kaon. The ratio of  $\bar{s}$  contribution in the kaon to the  $\bar{d}$  one in the pion given by  $F_{\bar{s}u\bar{s}}/F_{\bar{d}u\bar{d}}$  presents a dependence on  $Q^2$ , similar as we have discussed, i.e., it reflects the more compact configuration of the kaon with respect to the pion. We should say, that despite the large momentum behavior of the pion form factor for set (A) overestimate the experimental data, its prediction in lower momentum transfer region should be reasonable. As shown in the figure, the ratio between the  $\bar{s}$  and  $u$  contributions to the kaon form factor, namely  $e_{\bar{s}} F_{\bar{s}u\bar{s}}/(e_u F_{u\bar{s}u})$ , clearly is above the flavor symmetric value of  $1/2$  for larger momentum transfers as  $10 \text{ GeV}^2$ . Such an effect is quite visible in Fig. 5, when looking to the individual flavor contribution to the kaon charge form factor.

TABLE VI. Partial ratios for the electromagnetic form factors of pion (A) and kaon (C) at  $10 \text{ GeV}^2$ , compared with the NJL model from Ref. [36].

Model	$\frac{F_{u\bar{s}u}}{F_{u\bar{d}u}}$	$\frac{F_{\bar{s}u\bar{s}}}{F_{\bar{d}u\bar{d}}}$	$\frac{e_{\bar{s}} F_{\bar{s}u\bar{s}}}{e_u F_{u\bar{s}u}}$
This work	0.80	1.10	0.69
NJL [36]	0.36	2.74	0.56

In Table VI, the ratios of flavor form factors of the pion and kaon for the sets (A) and (C), respectively, and presented in Fig. 7 are compared with the results from the NJL model obtained in Ref. [36] at the particular value of  $Q^2 = 10 \text{ GeV}^2$ . The results in the table illustrate once more the SU(3) flavor symmetry breaking through the flavor form factor ratios. Our re-

TABLE VII. Ratio of the electromagnetic form factors for pion (A) and kaon (C), compared with calculations from [36, 66, 67] and experimental time-like data [68, 69].

Reference	$Q^2 \text{ [(GeV/c)}^2]$	$F_{\pi^+}/F_{K^+}$
This work	10.0	1.10
	13.48	1.14
	14.2	1.13
	17.4	1.16
Hutauruk et al. [36]	10.0	0.87
Bakulev et al. [66]	13.48	0.53
Shi et al. [67]	17.4	0.81
Pedlar et al. [68]	13.48	1.19(17)
Seth et al. [69]	14.2	1.21(3)
Seth et al. [69]	17.4	1.09(4)

sults show the deviation of  $F_{u\bar{s}u}/F_{u\bar{d}u}$  and  $F_{\bar{s}u\bar{s}}/F_{\bar{d}u\bar{d}}$  from unity, which are considerably smaller than in the NJL model reflecting that set (A) overestimates the pion form factor at large momentum. The results of the NJL model from Ref. [36] show a larger symmetry breaking for these ratios. The ratio between the  $\bar{s}$  and  $u$  flavor contributions to the kaon form factor (fourth column in Table VI) are consistent, even taking into account that quark current is dressed in Ref. [36], and in addition it shows that our Bethe-Salpeter model has a small, namely about 10%, flavor symmetry breaking for the up and strange quarks within the kaon. One important difference to be pointed out is that the NJL model as studied in Ref. [36], has infrared and ultraviolet scales, while our model is less flexible, having just one mass scale, which makes the present model more robust against flavor symmetry breaking among the quark contributions to the kaon form factor.

From the Phragmén-Lindelöf's theorem it follows that at large momentum transfers the asymptotic behavior of the form factors in the space-like and time-like regions must be the same [70, 71]. Therefore, in principle, we could compare our results for space like form factors at large momentum transfers with the experimental time-like ones [68, 69]. In Table VII, we present the ratios of  $F_{\pi^+}/F_{K^+}$  at some large  $Q^2$  values for our model calculated with sets (A) and (C), compared to results from other models [36, 66, 67]. In the flavor SU(3) symmetry limit, all the ratios presented in the table should be unity, which is clearly not the case. Furthermore, QCD predicts that for  $Q^2 \gg \Lambda_{QCD}$  the ratio between the form factors approaches  $f_\pi^2/f_K^2 \simeq 0.70$  [65], which suggests by com-

paring this ratio with the time-like experimental data, that  $Q^2 \sim 17 \text{ GeV}^2$  is still not in the asymptotic region. In particular our results for the ratio using set (A) and (C), for the pion and kaon respectively, overestimate the ratio, and if we had used instead set (B) for the pion we would have found a value below the unity, as the other models. We emphasize, that the parameter set (A) for the pion was chosen to analyze the pion, as it gives a better representation of the form factor at low momentum transfers, and in addition larger light quark masses of this set avoid to unbind the  $D^+$  and  $D_s^+$ , as we have already shown when discussing the static observables of these heavy-light mesons.

### B. $D^+$ and $D_s^+$ mesons

We study in what follows the  $D^+$  and  $D_s^+$  EM form factors and their flavor decomposition. In particular, we illustrate quantitatively the manifestation of the SU(4) flavor symmetry breaking on the contributions of each quark to the form factor. We have used the parameter sets (E) and (F) given in Table I, which fit the  $D^+$  and  $D_s^+$  decay constants, respectively. The masses of these heavy-light mesons are the experimental ones and given in the table. The comparison will be made with LQCD results of the form factors for  $D^+$  [17, 18] for  $D_s^+$  [18], even though the physical masses of these mesons were not achieved in these calculations. This has an impact on the charge radius, as it was verified in our discussion of Table IV. However taking into account the quoted errors of the lattice calculations our results are quite consistent with ensemble C1 used in Refs. [18]. Such a trend will be confirmed by comparing the form factors and the corresponding quark contributions with such LQCD results.

To have a phenomenological handle on the computed form factors, we exploit the VMD applied for  $D^+$  and  $D_s^+$ :

$$F_{D^+}(q^2) = \frac{2}{3} \frac{m_{J/\psi}^2}{m_{J/\psi}^2 - q^2} + \frac{1}{3} \frac{m_\rho^2}{m_\rho^2 - q^2}, \quad (35)$$

$$F_{D_s^+}(q^2) = \frac{2}{3} \frac{m_{J/\psi}^2}{m_{J/\psi}^2 - q^2} + \frac{1}{3} \frac{m_\phi^2}{m_\phi^2 - q^2}. \quad (36)$$

The expressions for the form factors based on the VMD where the masses of  $J/\Psi$ ,  $\rho$  and  $\phi$  determines the closest poles to the space-like momentum region in the photon-absorption amplitude. The values of the vector meson masses come from [16]. The VMD model form factor gives for  $D^+$  a charge radius of

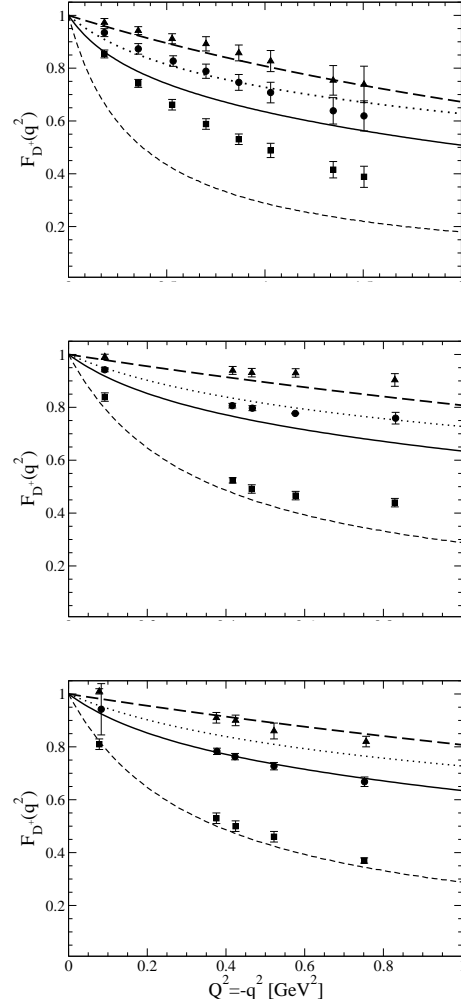


FIG. 8.  $D^+$  electromagnetic form factor with the corresponding quark contributions and comparison with lattice calculations. Our results:  $D^+$  form factor (full line),  $\bar{d}$  contribution -  $e_{\bar{d}}F_{\bar{d}c\bar{d}}$  (short-dashed line) and  $c$  contribution -  $e_cF_{c\bar{d}c}$  (dashed line). VMD (dotted line) from Eq. (35). LQCD results for  $D^+$  form factor (circles),  $\bar{d}$  contribution (squares) and  $c$  contribution (triangles). Upper panel: comparison with LQCD results from Ref. [17]. Middle panel: comparison with LQCD results from ensemble (B1) [18]. Lower panel: comparison with LQCD results from ensemble (C1) [18].

$r_{D^+} = 0.381 \text{ fm}$  and for  $D_s^+$  it gives  $r_{D_s^+} = 0.302 \text{ fm}$ . These values are somewhat close to the present model and also to the lattice results (see the Table III).

The results for the EM form factors of the  $D^+$  and  $D_s^+$  mesons are presented in Figs. 8 and 9, respec-



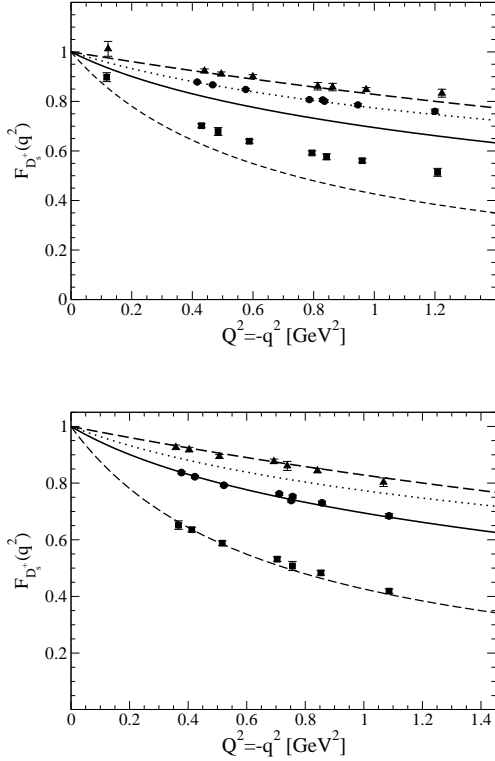


FIG. 9.  $D_s^+$  electromagnetic form factors with the corresponding quark contributions and comparison with lattice calculations. Our results:  $D_s^+$  form factor (full line),  $\bar{d}$  contribution (short-dashed line) and  $c$  contribution (dashed line), VMD (dotted line) from Eq. (35). LQCD results for  $D_s^+$  form factor (circles),  $\bar{s}$  contribution (squares) and  $c$  contribution (triangles). Upper panel: comparison with LQCD results from ensemble (B1) [18]. Lower panel: comparison with LQCD results from ensemble (C1) [18].

tively. In addition the flavor decomposition and the comparison with LQCD results from [17] and [18] are shown. The three panels of Fig. 8 are dedicated to the  $D^+$  form factor, where our calculations with parameter set (E) given in Table I, and the corresponding quark contributions, namely  $F_{\bar{d}c\bar{d}}$  and  $F_{c\bar{d}c}$ , are compared with LQCD results and the VMD model from Eq. (35). In the upper panel, the LQCD form factors [17] are shown together with the VMD, and set (E) models. As anticipated in the analysis of the charge radii in Table V we observe consistently that our model form factors are below the results from [17] up to  $2 \text{ GeV}^2$ .

The heavy quark contribution to the  $D^+$  form factor shown in Fig. 8 decreases slowly as it sits at the

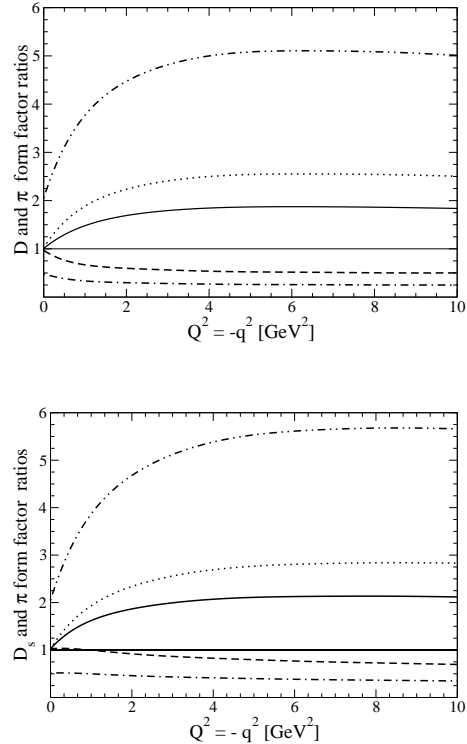


FIG. 10. The electromagnetic form factor ratios for the pion (A) and  $D$  mesons. Upper panel:  $F_{D^+}/F_{\pi^+}$  (solid line);  $F_{\bar{d}c\bar{d}}/F_{\bar{d}u\bar{d}}$  (dashed line);  $e_{\bar{d}}F_{\bar{d}c\bar{d}}/(e_u F_{\bar{d}u\bar{d}})$  (dot-dashed line);  $F_{c\bar{d}c}/F_{u\bar{d}u}$  (dotted line);  $e_c F_{c\bar{d}c}/(e_{\bar{d}} F_{\bar{d}u\bar{d}})$  (dot-dot-dashed line). Lower panel:  $F_{D^+}/F_{\pi^+}$  (solid line);  $F_{\bar{s}c\bar{s}}/F_{\bar{d}u\bar{d}}$  (dashed line);  $e_{\bar{s}}F_{\bar{s}c\bar{s}}/(e_u F_{\bar{d}u\bar{d}})$  (dot-dashed line);  $F_{c\bar{s}c}/F_{u\bar{d}u}$  (dotted line);  $e_c F_{c\bar{s}c}/(e_{\bar{d}} F_{\bar{d}u\bar{d}})$  (dot-dot-dashed line). The thin solid line is the reference for the SU(4) flavor symmetry.

center of mass of the meson, while the light quark form a "halo" charge distribution around the heavy quark, exploring the confinement region. Despite of that the behavior of  $F_{\bar{d}c\bar{d}}$  with  $Q^2$  is smooth making useful our model to represent the heavy-light meson charge distribution. The LQCD calculations from Ref. [18] were done with two ensembles, namely (B1) and (C1), with the last one providing the closest value of the  $D^+$  meson mass to the experimental value (see Table IV). These LQCD results are compared to our model, which are shown in the figure middle and lower panels. Up to the errors of the form factor computed with ensemble C1, we found agreement with our model, which does not happen with the VMD form factor. The light quark "halo" charge form fac-

tor from LQCD ensemble C1 is also reproduced, as well as the charm contribution to the  $D^+$  form factor.

In Fig. 9, we show results for the  $D_s^+$  electromagnetic form factor and the corresponding flavor decomposition for our model obtained with the parameter set (F). The comparison with VMD model and LQCD calculations from Ref. [18] with ensembles B1 (upper panel) and C1 (lower panel) is also shown. The form factor  $F_{D_s^+}$ , and flavor contributions  $F_{c\bar{s}c}$  and  $F_{\bar{s}c\bar{s}}$  underestimate the results from the LQCD ensembles B1, and the VMD model, are given in the upper panel of the figure. This result is expected as the computed radii are larger than the ones obtained with ensemble B1 (see Table V). The  $D_s^+$  form factor and its flavor content obtained with our model are in agreement with the outcomes from the lattice ensemble C1 as shown in the lower panel of the figure, a finding consistent with the one observed for  $D^+$  presented in the lower panel of Fig. 8. The consistency found for both  $D^+$  and  $D_s^+$  form factors and flavor content with the LQCD results from ensemble C1, suggests that the IR physics embedded within our parametrization and constituent masses reflect consistently the QCD long-distance effects in these heavy-light mesons. Important to observe that our choice of parametrization (A) for the pion and (C) for the kaon, describe both their charge radii and decay constants, quantities carrying the QCD nonperturbative IR physics.

In the following we discuss the manifestation of the SU(4) symmetry breaking in  $D^+$  and  $D_s^+$  form factors. For that aim in Fig. 10, we present several ratios of the electromagnetic form factors of the  $D$  mesons and their flavor components with the pion ones from model (A). In the upper panel, we present the ratio  $F_{D^+}/F_{\pi^+}$ , which tends to a value close to 2 for large momentum transfers. This ratio flattens above  $Q^2 = -q^2 \gtrsim 3 \text{ GeV}^2$  that indicates the momentum region where the difference in the constituent quark masses and values of the regulator scales  $\mu_M$  are somewhat irrelevant for the dependence on  $q^2$ , while the value of the ratio  $\sim 2$  seems to be more particular to our model. However, we should convey that the normalizations of the form factors are essentially determined at low momentum scales which should be more constrained with the fitting of the decay constant and charge radius. On the other hand, taking into account the ratio of decay constants squared the present value is about half of the value that it should be for  $F_{D_s^+}/F_{\pi^+}$  (lower panel), while for  $F_{D^+}/F_{\pi^+} \sim 2$  is consistent with that ratio.

The ratios of the  $\bar{d}$  contribution to the  $D^+$  and  $D_s^+$  to pion form factor, namely  $F_{\bar{d}c\bar{d}}/F_{\bar{d}u\bar{d}}$  (upper panel)

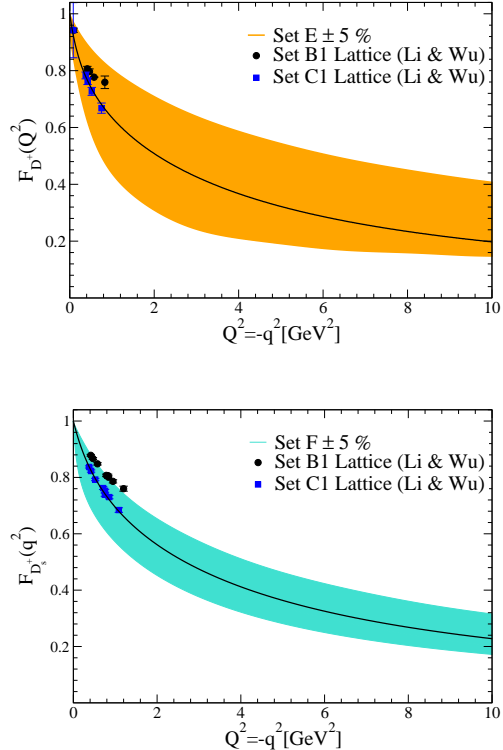


FIG. 11.  $D^+$  and  $D_s^+$  electromagnetic form factors, together with bands for parameter variations. Upper panel:  $D^+$  form factor band for set (E) with  $\pm 5\%$  variation of the model parameters. Lower panel:  $D_s^+$  form factor band for set (F) with  $\pm 5\%$  variation of the model parameters. For reference the LQCD results from ensembles B1 (circles) and C1 (squares) [18] are shown.

and  $F_{\bar{s}c\bar{s}}/F_{\bar{d}u\bar{d}}$  (lower panel), respectively, exemplify two aspects of the SU(4) flavor symmetry breaking, a strong one in the distribution of the  $\bar{d}$  charge in the  $D^+$ , which is extended with respect to the one in the pion, while the effect is somewhat weaker in the  $D_s^+$ , where the  $\bar{s}$  is heavier than  $\bar{d}$  and its charge distribution in  $D_s^+$  is similar to the pion one. This last observation is corroborated by the similar radii  $r_{D_s^+, \bar{s}}$  and  $r_\pi$  (see Tables I and V). The ratios  $e_{\bar{d}}F_{\bar{d}c\bar{d}}/(e_uF_{u\bar{d}u})$  (upper panel) and  $e_{\bar{s}}F_{\bar{s}c\bar{s}}/(e_uF_{u\bar{d}u})$  (lower panel) just reflect what we have already discussed. The heavy quark contribution to the  $D^+$  and  $D_s^+$  form factors and the associated evidence of SU(4) flavor symmetry breaking is clearly seen in the ratios  $F_{c\bar{d}c}/F_{u\bar{d}u}$  (upper panel) and  $F_{c\bar{s}c}/F_{u\bar{d}u}$  (lower panel), which saturate above  $\sim 3 \text{ GeV}^2$ , attaining a ratio about 3, in connection with the strong localization of the heavy

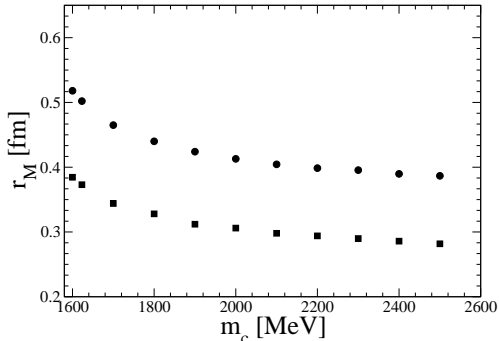


FIG. 12. Charge radii of  $D^+$  and  $D_s^+$  mesons as a function of the charm quark mass,  $m_c$ , having all other parameters fixed to set (E) for  $D^+$  (circles) and to set (F) for  $D_s^+$  (squares) .

quark at the meson center of mass. Such large ratio would be even increased if we had chosen a pion model that fits the form factor like model (B) at large momentum, and the flavor symmetry breaking would be even enhanced. These characteristics are visible in the ratios  $e_c F_{c\bar{d}c}/(e_{\bar{d}} F_{\bar{d}u\bar{d}})$  (upper panel) and  $e_c F_{c\bar{s}c}/(e_{\bar{d}} F_{\bar{d}u\bar{d}})$  (lower panel).

In Fig. 11, we show the effect of the variation of 5% in the parameters for both the form factors of  $D^+$  (upper panel) and  $D_s^+$  (lower panel). For reference, we include in the figure the LQCD results from [18]. The band width is larger for the case of  $D^+$  because it has a smaller binding energy, making the form factor much more sensitive to changes in the quark masses and regulator mass ( $\mu_M$ ), while for the  $D_s^+$  one observes a smaller band width. In both cases such parameter change is enough to englobe the LQCD results from ensembles B1 and C1 of Refs. [18], and for  $D^+$  also the calculations from Ref. [17] not shown in the figure.

Finally, to close our discussion we show in Fig. 12 the heavy-light meson charge radii obtained with the change of  $m_c$  while keeping the other parameters of set (E) and (F) fixed. The heavier the charm quark mass becomes, the charge radius of the  $D^+$  and  $D_s^+$  tends to saturate in a decreasing behavior and the main contribution comes from the light quark, which in our model perceives the minimum branch point value, namely,  $m_{\bar{d}(\bar{s})} + \mu_{D^+(D_s^+)} - m_{D^+(D_s^+)}$ , which is not affected by the increase of the charm mass and its corresponding localization. Such mechanism is particular to the present model, and mimics the realization of the heavy quark limit of QCD, where the center

of the confining force is fixed at the position of the heavy quark. In our case, such physics is simulated by keeping the lowest branch point fixed. However, it is necessary to distinguish that the present model, although baring some properties that QCD dictates to these heavy-light mesons, it does not posses the absolute confinement of the quarks.

## VI. SUMMARY

In the present work, the electroweak properties of light and charmed  $D$  and  $D_s$  pseudoscalar mesons are investigated within a unified covariant constituent quark model, where the quark-antiquark-meson vertices are assumed to have a symmetric form by the exchange of quark momenta, which were successful in describing the light pseudoscalar meson properties [20, 22]. The model has constituent quark masses up, down, strange and charm, which embody dynamical chiral symmetry breaking and the Higgs contribution to the masses. In addition, each meson has one mass regulator parameter tuned to reproduce the weak decay constant. Consistently with the infrared relevance of the dynamical chiral symmetry breaking, we chose a light quark constituent mass that reproduces the pion charge radius, even loosing fit at large momentum of the experimental form factor data.

The reason for such a choice was to study the kaon,  $D^+$ ,  $D_s^+$  electromagnetic form factors at low space-like momentum transfer squared up to about  $1 \text{ GeV}^2$ , where experimental data for the kaon is available [14, 15], as well as lattice calculations for the  $D^+$  [17, 18] and  $D_s^+$  [18]. In particular, we gave attention to the SU(3) and SU(4) flavor symmetry breaking as a consequence of the Higgs contribution to the quark masses, where from the LQCD calculations also provide the flavor decomposition of these heavy-light meson form factors. Furthermore, we have compared our charge radius results with some models from the literature, which can be useful for contextualizing our effort within what has been done. The charge distribution of  $\bar{s}$  is somewhat more compact than the corresponding one for the  $u$ , a feature that will be strongly emphasized for the charmed heavy-light pseudoscalars.

Each of the form factors were decomposed in its flavor content,  $F_{u\bar{d}u}(q^2)$  and  $F_{\bar{d}u\bar{d}}(q^2)$  for the pion,  $F_{u\bar{s}u}(q^2)$  and  $F_{\bar{s}u\bar{s}}(q^2)$  for the kaon,  $F_{c\bar{d}c}(q^2)$  and  $F_{\bar{d}c\bar{d}}(q^2)$  for  $D^+$ ,  $F_{c\bar{s}c}(q^2)$  and  $F_{\bar{s}c\bar{s}}(q^2)$  for the  $D_s^+$ . Each of these flavor form factors has particular properties with respect to the flavor symmetry. The model

has SU(2) flavor symmetry and trivially we have  $F_{u\bar{d}u}(q^2) = F_{\bar{d}u\bar{d}}(q^2) = F_{\pi^+}(q^2)$ , which we used constituent quark mass that reproduced quite well the pion charge radius, favoring a better description of the infrared properties of the model. The SU(3) flavor symmetry is slightly broken within the kaon expressed by  $F_{s\bar{u}s}(q^2) \gtrsim F_{u\bar{s}u}(q^2)$  by about 10% above  $3 \text{ GeV}^2$ , as consequence of the Higgs contribution to the strange quark, which makes it about 30% heavier than the up quark in our model. The study of the flavor contribution to the  $D^+$  and  $D_s^+$  form factors within the model, showed that the charm quark is localized close to the center of the meson, while the light quark forms a "halo" exploring larger distances where the confining force of QCD is active, and the infrared physics dominating. Such strong asymmetry is a direct consequence of the Higgs providing a large mass to the charm quark in comparison with light ones. The flavor decomposition of the charge radii provided by the model is consistent with the lattice QCD calculation from Refs. [18] where the ensemble C1 was used, and the  $D^+$  and  $D_s^+$  masses were found close to the experimental values.

We found that the heavier is the charm quark, the charge radius of the  $D^+$  and  $D_s^+$  decrease and saturates, as dominant contribution to the charge radius comes from the light quark. The contribution of the light quark to the heavy-light form factor is essentially dependent on the minimum branch point value at  $m_{\bar{d}(\bar{s})} + \mu_{D^+(D_s^+)} - m_{D^+(D_s^+)}$ , which is insensitive to the increase of the charm quark mass, and its corresponding localization. Such feature is particular to the present model, and is able to incorporate aspects of the heavy quark limit of QCD, where the force center of the confining force stays at the meson center of mass, and therefore the charge distribution becomes independent of the heavy quark mass.

However, the present model does not possess the absolute confinement of the quarks, and they are represented as bound states of constituents quarks. The SU(4) flavor symmetry is largely broken as manifested in the contributions to the form factors, where we found in the case of the  $D^+$  that  $F_{c\bar{d}c}(q^2) > F_{\bar{d}c\bar{d}}(q^2)$  and saturating the ratio above  $3 \text{ GeV}^2$ , attaining the ratio a value  $\sim 5$ . For the  $D_s^+$ , we observe the same behavior as for the  $D^+$  having that  $F_{c\bar{s}c}(q^2) > F_{\bar{s}c\bar{s}}(q^2)$  and the ratio saturating at a value around 5 above  $3 \text{ GeV}^2$ . This is a strong manifestation of the SU(4) flavor symmetry breaking in the structure of these heavy-light pseudoscalar mesons. We also found that the flavor decomposition of the  $D^+$  and  $D_s^+$  form factors are in agreement with the lattice QCD calculation from Refs. [18] where the ensemble C1 was used, with results in the space-like region up to  $1.2 \text{ GeV}^2$ . The structure of the  $D^+$  and  $D_s^+$  mesons can be studied in much more detail within this model, like for generalized parton distributions, generalized transverse momentum distributions and finally fragmentation functions of the heavy quarks, left for future investigations as well as the application of the model to study  $B, \eta_c, J/\psi, \eta_b$  and  $\Upsilon$  mesons.

*Acknowledgements:* This work was supported in part by CAPES, and by the Conselho Nacional de Desenvolvimento Científico e Tecnológico (CNPq), Grants, No. 308486/2015-3 (TF), Process, No. 307131/2020-3 (JPBCM), Process, No. 313063/2018-4 (KT), and No. 426150/2018-0 (KT), and Fundação de Amparo à Pesquisa do Estado de São Paulo (FAPESP), Process, No. 2019/02923-5 (JPBCM), No. 2019/00763-0 (KT), and was also part of the projects, Instituto Nacional de Ciência e Tecnologia – Nuclear Physics and Applications (INCT-FNA), Brazil, Process No. 464898/2014-5, and FAPESP Temático, Brazil, Process, the thematic projects, No. 2013/26258-4 and No. 2017/05660-0.

- 
- [1] T. Horn and C. D. Roberts, *J. Phys. G* **43**, 073001 (2016), [arXiv:1602.04016 \[nucl-th\]](#).
  - [2] A. C. Aguilar *et al.*, *Eur. Phys. J. A* **55**, 190 (2019), [arXiv:1907.08218 \[nucl-ex\]](#).
  - [3] N. Brambilla *et al.*, *Eur. Phys. J. C* **71**, 1534 (2011), [arXiv:1010.5827 \[hep-ph\]](#).
  - [4] H.-X. Chen, W. Chen, X. Liu, Y.-R. Liu, and S.-L. Zhu, *Rep. Prog. Phys.* **80**, 076201 (2017).
  - [5] B. L. G. Bakker *et al.*, *Nucl. Phys. B Proc. Suppl.* **251-252**, 165 (2014), [arXiv:1309.6333 \[hep-ph\]](#).
  - [6] O. Oliveira, P. J. Silva, J.-I. Skullerud, and A. Sternbeck, *Phys. Rev. D* **99**, 094506 (2019).
  - [7] M. Y. Khlopov, *Sov. J. Nucl. Phys.* **28**, 583 (1978), *.Yad.Fiz.* **28**, 1134 (1978).
  - [8] M. Neubert, *Phys. Rept.* **245**, 259 (1994).
  - [9] R. Baldini, S. Dubnička, P. Gauzzi, S. Pacetti, E. Pasqualucci, and Y. Srivastava, *Nucl. Phys. A* **666**, 38 (2000).
  - [10] J. Volmer, D. Abbott, H. Anklin, C. Armstrong, J. Arrington, K. Assamagan, S. Avery, O. Baker, H. Blok,

- C. Bochna, *et al.*, *Phys. Rev. Lett.* **86**, 1713 (2001).
- [11] T. Horn, K. Aniol, J. Arrington, B. Barrett, E. Beise, H. Blok, W. Boeglin, E. Brash, H. Breuer, C. Chang, *et al.*, *Phys. Rev. Lett.* **97**, 192001 (2006).
- [12] V. Tadevosyan, H. Blok, G. Huber, D. Abbott, H. Anklin, C. Armstrong, J. Arrington, K. Assamagan, S. Avery, O. Baker, *et al.*, *Phys. Rev. C* **75**, 055205 (2007).
- [13] G. Huber, H. Blok, T. Horn, E. Beise, D. Gaskell, D. Mack, V. Tadevosyan, J. Volmer, D. Abbott, K. Aniol, *et al.*, *Phys. Rev. C* **78**, 045203 (2008).
- [14] E. B. Dally *et al.*, *Phys. Rev. Lett.* **45**, 232 (1980).
- [15] S. R. Amendolia *et al.*, *Phys. Lett. B* **178**, 435 (1986).
- [16] P. A. Zyla *et al.* (Particle Data Group), *PTEP* **2020**, 083C01 (2020).
- [17] K. U. Can, G. Erkol, M. Oka, A. Ozpineci, and T. T. Takahashi, *Phys. Lett. B* **719**, 103 (2013), [arXiv:1210.0869 \[hep-lat\]](#).
- [18] N. Li and Y.-J. Wu, *Eur. Phys. J. A* **53**, 56 (2017).
- [19] C. Itzykson and J.-B. Zuber, *Quantum field theory* (Courier Corporation, 2012), McGraw-Hill, New York, International Series In Pure and Applied Physics, ISBN 978-0-486-44568-7.
- [20] J. P. B. C. de Melo, T. Frederico, E. Pace, and G. Salmè, *Nucl. Phys. A* **707**, 399 (2002), [arXiv:nucl-th/0205010](#).
- [21] B. El-Bennich, J. P. B. C. de Melo, B. Loiseau, J. P. Dedonder, and T. Frederico, *Braz. J. Phys.* **38**, 465 (2008), [arXiv:0805.0768 \[hep-ph\]](#).
- [22] G. H. S. Yabusaki, I. Ahmed, M. A. Paracha, J. P. B. C. de Melo, and B. El-Bennich, *Phys. Rev. D* **92**, 034017 (2015), [arXiv:1504.06764 \[hep-ph\]](#).
- [23] T. Frederico and G. Salmè, *Few-Body Syst.* **49**, 163 (2011), [arXiv:1011.1850 \[nucl-th\]](#).
- [24] C. Mezrag, H. Moutarde, and J. Rodriguez-Quintero, *Few-Body Syst.* **57**, 729 (2016), [arXiv:1602.07722 \[nucl-th\]](#).
- [25] C. Fanelli, E. Pace, G. Romanelli, G. Salmè, and M. Salmistraro, *Eur. Phys. J. C* **76**, 253 (2016), [arXiv:1603.04598 \[hep-ph\]](#).
- [26] W. de Paula, E. Ydrefors, J. H. Alvarenga Nogueira, T. Frederico, and G. Salmè, *Phys. Rev. D* **103**, 014002 (2021), [arXiv:2012.04973 \[hep-ph\]](#).
- [27] S. Mandelstam, *Proc. Roy. Soc. Lond. A* **233**, 248 (1955), doi: 10.1098/rspa.1955.0261.
- [28] F. E. Close, *An Introduction to Quarks and Partons* (1979), Academic Press, London, New York, San Francisco, ISBN 978-0-12-175152-4.
- [29] Z. W. Lin, C. M. Ko, and B. Zhang, *Phys. Rev. C* **61**, 024904 (2000), [arXiv:nucl-th/9905003](#).
- [30] M. E. Bracco, M. Chiapparini, F. S. Navarra, and M. Nielsen, *Prog. Part. Nucl. Phys.* **67**, 1019 (2012), [arXiv:1104.2864 \[hep-ph\]](#).
- [31] H. Georgi, *Weak Interactions and Modern Particle Theory* (1984), The Benjamin/Cummings Publishing Company, Inc., Advanced Book Program (1984), Menlo Park, California, ISBN 978-0-8053-3163-9.
- [32] P. Maris and P. C. Tandy, *Phys. Rev. C* **62**, 055204 (2000), [arXiv:nucl-th/0005015](#).
- [33] G. Lepage and S. J. Brodsky, *Phys. Rev. D* **22**, 2157 (1980).
- [34] M. Ablikim *et al.* (BESIII), *Phys. Rev. Lett.* **122**, 071802 (2019), [arXiv:1811.10890 \[hep-ex\]](#).
- [35] L. A. M. Salcedo, J. P. B. C. de Melo, D. Hadjmichef, and T. Frederico, *Braz. J. Phys.* **34**, 297 (2004), [arXiv:hep-ph/0311008](#).
- [36] P. T. P. Hutaaruk, I. C. Cloët, and A. W. Thomas, *Phys. Rev. C* **94**, 035201 (2016), [arXiv:1604.02853 \[nucl-th\]](#).
- [37] E. F. Suisso, J. P. B. C. de Melo, and T. Frederico, *Phys. Rev. D* **65**, 094009 (2002), [arXiv:hep-ph/0202137](#).
- [38] S. J. Brodsky, H.-C. Pauli, and S. S. Pinsky, *Phys. Rept.* **301**, 299 (1998), [arXiv:hep-ph/9705477 \[hep-ph\]](#).
- [39] J. P. C. B. de Melo, H. W. L. Naus, and T. Frederico, *Phys. Rev. C* **59**, 2278 (1999), [arXiv:hep-ph/9710228](#).
- [40] B. L. G. Bakker, H.-M. Choi, and C.-R. Ji, *Phys. Rev. D* **63**, 074014 (2001), [arXiv:hep-ph/0008147](#).
- [41] A. Faessler, T. Gutsche, M. A. Ivanov, V. E. Lyubovitskij, and P. Wang, *Physical Review D* **68** (2003), 10.1103/physrevd.68.014011.
- [42] D. Ebert, R. N. Faustov, and V. O. Galkin, *Phys. Lett. B* **635**, 93 (2006), [arXiv:hep-ph/0602110](#).
- [43] D. Ebert, R. N. Faustov, and V. O. Galkin, *Eur. Phys. J. C* **47**, 745 (2006), [arXiv:hep-ph/0511029](#).
- [44] A. Bashir, L. Chang, I. C. Cloët, B. El-Bennich, Y.-X. Liu, C. D. Roberts, and P. C. Tandy, *Commun. Theor. Phys.* **58**, 79 (2012), [arXiv:1201.3366 \[nucl-th\]](#).
- [45] M. Chen and L. Chang, *Chin. Phys. C* **43**, 114103 (2019), [arXiv:1903.07808 \[nucl-th\]](#).
- [46] M. A. Ivanov, J. G. Körner, J. N. Pandya, P. Santorelli, N. R. Soni, and C.-T. Tran, *Front. Phys. (Beijing)* **14**, 64401 (2019), [arXiv:1904.07740 \[hep-ph\]](#).
- [47] E. O. da Silva, J. P. B. C. de Melo, B. El-Bennich, and V. S. Filho, *Phys. Rev. C* **86**, 038202 (2012), [arXiv:1206.4721 \[nucl-th\]](#).
- [48] S. Jia and J. P. Vary, *Phys. Rev. C* **99**, 035206 (2019), [arXiv:1811.08512 \[nucl-th\]](#).

- [49] H.-M. Choi, *Phys. Rev. D* **75**, 073016 (2007), [arXiv:hep-ph/0701263](#).
- [50] C.-W. Hwang, *Phys. Rev. D* **81**, 054022 (2010), [arXiv:0910.0145 \[hep-ph\]](#).
- [51] T. Das, D. K. Choudhury, and K. K. Pathak, *Indian J. Phys.* **90**, 1307 (2016), [arXiv:1505.05634 \[hep-ph\]](#).
- [52] N. Dhiman and H. Dahiya, *Eur. Phys. J. Plus* **133**, 134 (2018), [arXiv:1708.07274 \[hep-ph\]](#).
- [53] S. Tang, Y. Li, P. Maris, and J. P. Vary, *Eur. Phys. J. C* **80**, 522 (2020), [arXiv:1912.02088 \[nucl-th\]](#).
- [54] C. Aubin *et al.*, *Phys. Rev. Lett.* **95**, 122002 (2005), [arXiv:hep-lat/0506030](#).
- [55] E. Follana, C. T. H. Davies, G. P. Lepage, and J. Shigemitsu (HPQCD, UKQCD), *Phys. Rev. Lett.* **100**, 062002 (2008), [arXiv:0706.1726 \[hep-lat\]](#).
- [56] W.-P. Chen, Y.-C. Chen, T.-W. Chiu, H.-Y. Chou, T.-S. Guu, and T.-H. Hsieh (TWQCD), *Phys. Lett. B* **736**, 231 (2014), [arXiv:1404.3648 \[hep-lat\]](#).
- [57] N. Carrasco *et al.*, *Phys. Rev. D* **91**, 054507 (2015), [arXiv:1411.7908 \[hep-lat\]](#).
- [58] R. Tarrach, *Z. Phys. C* **2**, 221 (1979).
- [59] S. B. Gerasimov, *Yad. Fiz.* **29**, 513 (1979), [Erratum: *Sov.J.Nucl.Phys.* 32, 156 (1980), Erratum: *Yad.Fiz.* 32, 304 (1980)].
- [60] R. Trotta, T. Horn, and A. Vargas, in *APS Division of Nuclear Physics Meeting Abstracts*, APS Meeting Abstracts, Vol. 2017 (2017) p. CF.004.
- [61] J. J. Sakurai, *Annals Phys.* **11**, 1 (1960).
- [62] J. J. Sakurai, *Currents and Mesons* (University of Chicago Press, 1969).
- [63] H. B. O'Connell, B. C. Pearce, A. W. Thomas, and A. G. Williams, *Prog. Part. Nucl. Phys.* **39**, 201 (1997), [arXiv:hep-ph/9501251](#).
- [64] C. S. Mello, J. P. B. C. de Melo, and T. Frederico, *Phys. Lett. B* **766**, 86 (2017).
- [65] G. Lepage and S. J. Brodsky, *Phys. Lett. B* **87**, 359 (1979).
- [66] A. P. Bakulev, S. V. Mikhailov, and N. G. Stefanis, *Phys. Lett. B* **508**, 279 (2001), [Erratum: *Phys.Lett.B* 590, 309–310 (2004)], [arXiv:hep-ph/0103119](#).
- [67] C. Shi, L. Chang, C. D. Roberts, S. M. Schmidt, P. C. Tandy, and H.-S. Zong, *Phys. Lett. B* **738**, 512 (2014), [arXiv:1406.3353 \[nucl-th\]](#).
- [68] T. K. Pedlar *et al.* (CLEO), *Phys. Rev. Lett.* **95**, 261803 (2005), [arXiv:hep-ex/0510005](#).
- [69] K. K. Seth, S. Dobbs, Z. Metreveli, A. Tomaradze, T. Xiao, and G. Bonvicini, *Phys. Rev. Lett.* **110**, 022002 (2013), [arXiv:1210.1596 \[hep-ex\]](#).
- [70] S. M. Bilenky, C. Giunti, and V. Wataghin, *Z. Phys. C* **59**, 475 (1993), [arXiv:hep-ph/9304221](#).
- [71] A. Denig and G. Salmè, *Prog. Part. Nucl. Phys.* **68**, 113 (2013), [arXiv:1210.4689 \[hep-ex\]](#).